[American Journal of Science, Vol. 307, January, 2007, P. 168–215, DOI 10.2475/01.2007.06]

ORIGIN OF THE LYME DOME AND IMPLICATIONS FOR THE TIMING OF MULTIPLE ALLEGHANIAN DEFORMATIONAL AND INTRUSIVE EVENTS IN SOUTHERN CONNECTICUT

GREGORY J. WALSH*†, JOHN N. ALEINIKOFF**, and ROBERT P. WINTSCH***

ABSTRACT. Geologic mapping, structural analysis, and geochronology in the area of the Lyme dome, southern Connecticut provides constraints on the origin of the rocks in the core of the dome, the absolute timing of the principal deformational and thermal events attributed to Alleghanian orogenesis, and the processes that generated the dome. Detrital zircon geochronology in combination with ages on intrusive rocks brackets the deposition of quartzite in the core of the dome sometime between ca. 925 and 620 Ma. Granite and granodiorite intruded the Neoproteorozic metasedimentary rocks in the core of the dome at ca. 620 to 610 Ma. Four major early Permian events associated with the Alleghanian orogeny affected the rocks in the Lyme dome area. Syn-tectonic migmatization and widespread penetrative deformation (D1, ca. 300 – 290 Ma) included emplacement of alaskite at 290 ± 4 Ma during regional foliation development and aluminosilicate-orthoclase metamorphic conditions. Rocks of the Avalon terrane may have wedged between Gander cover rocks and Gander basement in the core of the Lyme during D1. Limited structural evidence for diapiric uplift of the Lyme dome indicates that diapirism started late in D1 and was completed by D2 (ca. 290 – 280 Ma) when horizontal WNW contractional stresses dominated over vertical stresses. Second sillimanite metamorphism continued and syn-tectonic D2 granite pegmatite (288 ± 4 Ma) and the Joshua Rock Granite Gniess (284 ± 3 Ma) intruded at this time. North-northwest extension during D3 (ca. 280 – 275 Ma) led to granitic pegmatite intrusion along S3 cleavage planes and in extensional zones in boudin necks during hydraulic failure and decompression melting. Intrusion of a Westerly Granite dike at 275 ± 4 Ma suggests that D3 extension was active, and perhaps concluding, by ca. 275 Ma. Late randomly oriented but gently dipping pegmatite dikes record a final stage of intrusion during D4 (ca. 275 – 260 Ma), and a switch from NNW extension to vertical unloading and exhumation. Monazite and metamorphic zircon rim ages record this event at ca. 259 Ma. The evolution of the Lyme dome involved D1 mylonitization, intrusion, and migmatization during north-directed contraction, limited late D1 diapirism, D2 migmatization during WNW contraction with associated flexural flow and fold interference, D3 NNW horizontal extension and decompression melting, and final D4 vertical extension and rapid exhumation. Late regional uplift, extension, and normal faulting at higher crustal levels may have been caused by diapiric rise of the lower crust, below the structural level of the Lyme dome. The rocks record no evidence of Acadian metamorphism or deformation, suggesting that the Gander zone here was not tectonically juxtaposed with Avalon until the Alleghanian orogeny.

INTRODUCTION

In coastal Connecticut, new Pb and Nd isotopic data has identified crust of the Gander terrane in the core of the Lyme dome in an area long considered part of the Avalon terrane (figs. 1, 2; Wintsch and others, 2005a; Aleinikoff and others, 2007). Although the basement rocks in the Gander and Avalon terranes have overlapping Neoproterozoic ages (van Staal, 2005), their different sources for their igneous rocks leads to significant differences in isotope geochemistry. Felsic igneous rocks in the Gander terrane generally have negative initial ε_{Nd} and relatively high $^{207}Pb/^{204}Pb$ ratios as compared to similar rocks in the Avalon terrane which have positive initial ε_{Nd}

*U. S. Geological Survey, 87 State Street Room 324, Montpelier, Vermont 05602
**U. S. Geological Survey, Box 25046, MS 963, Denver, Colorado 80225
***Indiana University, Department of Geological Sciences, Bloomington, Indiana 47405
†Corresponding author: gwalsh@usgs.gov

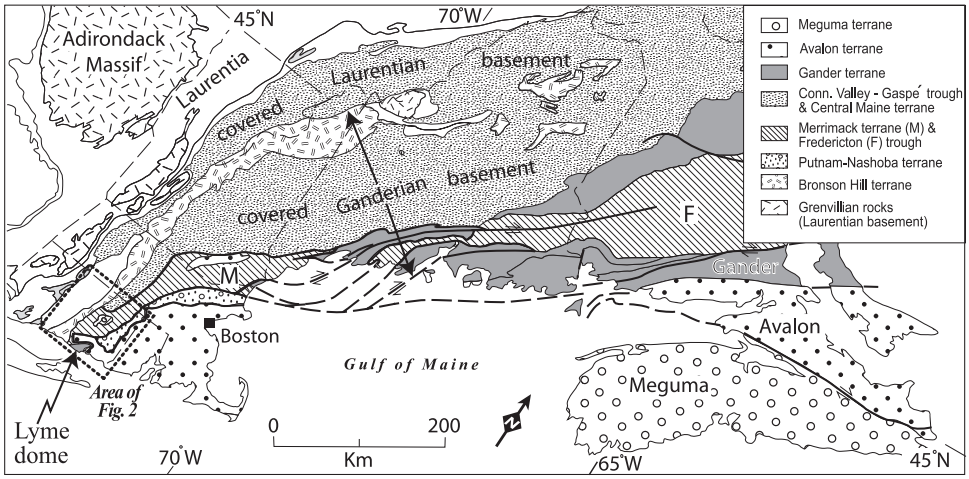

Fig. 1. Generalized tectonic map of the northern Appalachians in New England and Canada showing the location of the Lyme dome (adapted from Rankin and others, 2007).

and relatively low $^{207}Pb/^{204}Pb$ due to a greater component of a more primitive source (Barr and Hegner, 1992; Kerr, 1993; Whalen and others, 1994; van Staal and others, 1996; Aleinikoff and others, 2007). This discovery of Gander zone rocks in the Lyme dome is critical to testing the continuity of terranes and the timing of terrane accretion throughout the northern Appalachians. In Maritime Canada, the arrival of the Gander zone is thought to be responsible for the Silurian Salinic Orogeny, whereas accretion of the Avalon block supposedly caused the Acadian Orogeny by further shortening of Gander against Laurentia (for example, van Staal, 2005). In contrast, evidence from rocks of southern New England suggests that the Avalon terrane was not juxtaposed against the Gander and Laurentian terranes until the Carboniferous to Permian, during the late Paleozoic Alleghanian Orogeny (Gromet, 1989; Getty and Gromet, 1992; Wintsch and others, 1992, 2003, 2005b).

Early work by Dixon and Lundgren (1968) recognized that the tectonic history of eastern and southeastern Connecticut involved isoclinal folding associated with mylonitization and thrust faulting, high-grade metamorphism, doming, and later extensional faulting and intrusion. Lundgren and Ebblin (1972) noted that the time of formation of the Lyme dome post-dated mylonitization in the Honey Hill – Lake Char fault, a major tectonic boundary at the top of the Avalon terrane (fig. 2). Dixon and Lundgren (1968) also recognized that the timing of the major phases of tectonic activity were not well constrained. Lundgren (1966a, 1967) identified syn-tectonic peak metamorphic events associated with sillimanite-orthoclase and sillimanite-muscovite assemblages and migmatization and subsequent post-tectonic garnet replacement in the core of the Lyme dome. He interpreted these events as Permian or older, but pointed out the difficulty in distinguishing the age relationships between tectonic, metamorphic, and intrusive events.

Later work (Goldsmith, 1985a; Zartman and Hermes, 1987; Zartman and others, 1988) advanced our knowledge of the timing of tectonic and intrusive events in southern Connecticut by showing that the Joshua Rock Granite Gneiss was Late Pennsylvanian to Permian (not Neoproterozoic), that it was deformed during doming, and that Permian Westerly Granite dikes and Narragansett Pier Granite post-dated older deformational fabrics. O'Hara and Gromet (1983) showed Permian ages for retrograde greenschist facies metamorphism in the Honey Hill –Lake Char fault zone. Goldsmith (1985a, 1988), however, acknowledged that the timing of older, pre-dome

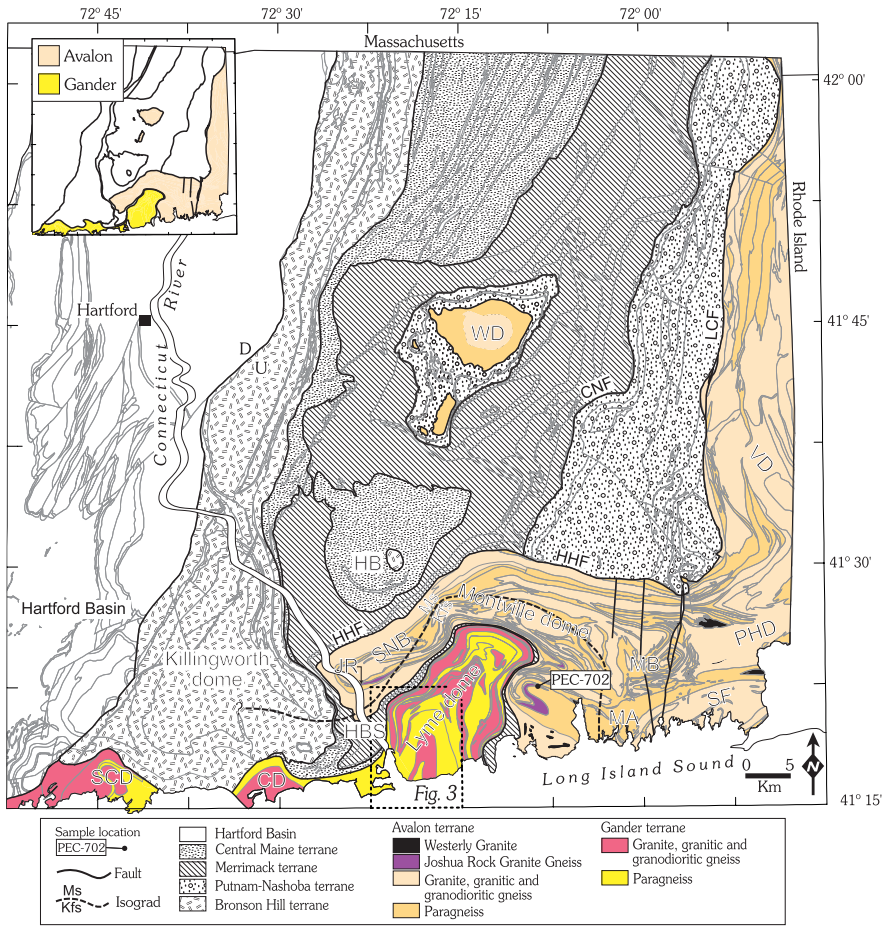

Fig. 2. Generalized tectonic map of eastern Connecticut showing the distribution of terranes and major Alleghanian domes and basins (modified after Rodgers, 1985; and Goldmith, 1985a). Sample locality PEC-702 in the Joshua Rock Granite Gneiss is from Zartman and others (1988). Upper left inset map shows the distribution of the Gander and Avalon terranes. Abbreviations: LCF - Lake Char fault, CNF – Clinton-Newbury fault, HHF – Honey Hill fault, WD - Willimantic dome, HB – Hopyard basin, HBS - Hunts Brook slice, SCD – Stony Creek dome, CD – Clinton dome, SNB – Selden Neck block, MA – Mystic antiform, MB - Mystic basin, SF – Stonington fold, PHD – Potter Hill dome, VD – Voluntown dome, JR – Joshua Rock, and Ms – muscovite and Kfs – potassium feldspar along the second sillimanite isograd.

stage deformation, including isoclinal folding and foliation development, was not clear, but that younger deformation of the rocks of the New London anticlinorium (fig. 2) included rapid uplift and tilting in the Permian.

In this study we present new geochronology and structural data for Neoproterozoic and late Paleozoic rocks from southern Connecticut to derive a tectonic model for the evolution of the Lyme dome. This study presents comprehensive evidence that links the absolute and relative timing of Alleghanian deformational and thermal events including anatexis, dome formation, and widespread decompression melting.

GEOLOGIC SETTING

The Lyme dome of southern Connecticut exposes migmatitic Neoproterozoic and Pennsylvanian-Permian gneiss and granite in a sequence of thrust nappes (for example, Wintsch and others, 1990, 1992). Neoproterozoic rocks of the Avalon terrane are

separated from overlying rocks by the Honey Hill-Lake Char fault system (fig. 2). Rocks of the Avalon terrane are restricted to the Selden Neck block, Montville dome, Potter Hill dome, Mystic basin, Stonington fold, and Voluntown dome (fig. 2). Regionally, the Selden Neck block, Montville dome, and Potter Hill dome form the New London anticlinorium (Goldsmith, 1985a). Rocks of the Avalon terrane are structurally overlain by the Silurian and older rocks of the Putnam-Nashoba terrane, and capped by the Merrimack and Central Maine terranes (fig. 2). Lead and Nd isotopic data now indicate that rocks in the Lyme dome are part of the Gander terrane (Wintsch and others, 2005a; Aleinikoff and others, 2007). They are separated from the structurally overlying Avalonian rocks by a tectonic belt including Merrimack terrane rocks in the Hunts Brook slice (fig. 2). Lundgren (1967) and Rodgers (1985) used the term Hunts Brook syncline for the structure between the Lyme dome and the Selden Neck block (fig. 2) based on inferred stratigraphic symmetry. With the recognition of distinct Avalon and Gander terranes, that stratigraphic symmetry no longer exists, and we use the term Hunts Brook slice because the Merrimack terrane rocks are either entirely fault-bounded, or they may have been deposited on Gander basement and over-ridden by Avalon.

The Lyme dome is part of an unevenly spaced, non-linear array of gneiss domes (Yin, 2004) in southern Connecticut (fig. 2). Only the northern end of the Lyme dome is exposed; the southern end is buried beneath glacial deposits (Stone and others, 2005) and submerged beneath Long Island Sound (fig. 2). Aeromagnetic data suggest that rocks in the Lyme dome continue offshore about half way across the sound, and may be contiguous with rocks in the Clinton dome (Zeitz and others, 1974, 1980; Daniels and Snyder, 2004). Neoproterozoic gneisses in the southern Connecticut gneiss dome belt are subdivided into layered paragneisses and plutonic orthogneisses. Permian plutonic rocks occur as deformed or post-tectonic intrusive bodies throughout the Neoproterozoic gneisses (fig. 2). Most of the Permian plutonic rocks intrude the Neoproterozoic gneisses south and east of the Lake Char – Honey Hill fault system (fig. 2) (Lundgren and others, 1958; Lundgren, 1963; Dixon and Lundgren, 1968; Lundgren and Ebblin, 1972; Losh and Bradbury, 1984; Rodgers, 1985; Gromet, 1989; Goldstein, 1992, 1994, 1998). Many workers recognized that the high-grade gneissic rocks south and east of the Lake Char – Honey Hill fault system were metamorphosed only in the late Paleozoic Alleghanian orogeny (Lundgren, 1966a; Dixon and Lundgren, 1968; Dallmeyer, 1982; Goldsmith, 1985a; Wintsch and Aleinikoff, 1987; Zartman and Hermes, 1987; Gromet, 1989; Wintsch and others, 1992, 1993, 2003; Gromet and others, 1998). In southern Connecticut, metamorphic temperatures exceeded 650° to 700° C, and migmatites formed during partial melting of metasedimentary rocks initiated in part by early muscovite-out reactions at the exposed structural level and biotite-out reactions at depth (Lundgren, 1966a; McLellan and Stockman, 1985; McLellan and others, 1993; Wintsch and others, 2003). Locally, metamorphic conditions reached 730° C and 6.5 kbar (McLellan and others, 1993). Thus, the late Paleozoic Alleghanian orogenic event is considered to have been responsible for the majority of deformation, dome formation, metamorphism, and intrusion in this area. Geologic questions that remain include (1) the origin of the protoliths of the gneisses in the core of the Lyme dome, (2) the absolute timing of the principal deformational and thermal events attributed to Alleghanian orogenesis, and (3) the processes that generated the Lyme dome.

Regional metamorphic studies have created a framework for the timing of Alleghanian tectono-thermal events. Structural and isotopic studies around the Willimantic dome (Wintsch, 1979; Getty and Gromet, 1992; Wintsch and others, 1992) indicate that the tectonic cover rocks experienced Acadian metamorphism at ca. 405 to 403 Ma, whereas Avalonian core rocks in the dome only experienced Pennsylvanian through Permian thermal events. Getty and Gromet (1992) and Wintsch and others

(1993) proposed that the Avalonian rocks were thrust under the cover rocks during convergence around 305 to 290 Ma, experienced melting at 285 to 270 Ma, and later extensional faulting at 280 to 265 Ma. More recent isotopic work and conventional U-Pb geochronology from zircon, monazite, and sphene led Gromet and others (1998) to apply the model of Getty and Gromet (1992) to southeastern New England. This general model includes early high-grade ductile deformation at ca. 305 to 290 Ma, felsic magmatism during partial melting at ca. 280 to 270 Ma, and finally extensional collapse at ca. 280 to 260 Ma. Wintsch and others (2003) reported new constraints on the timing of peak Alleghanian metamorphism in the Bronson Hill terrane of Connecticut from U-Pb ages from metamorphic sphene and $^{40}Ar/^{39}Ar$ ages from amphibole and muscovite. The new ages indicate peak temperatures in northern Connecticut occurred at ca. 305 to 294 Ma (Pennsylvanian to Early Permian) whereas to the south, peak metamorphism occurred in the Late Permian. Wintsch and others (2003) concluded that the Avalon and Bronson Hill terranes achieved thermal equilibrium by the early Permian, major motion between the two terranes had ended by the middle Permian, and thermal effects lasted into the late Permian.

RESULTS

Geologic mapping, structural analysis, and geochronology were conducted in the area of the Lyme dome. Recent mapping in the Old Lyme quadrangle in Connecticut (fig. 3; Walsh and others, 2006) has redefined the structure and distribution of the Neoproterozoic to Silurian metasedimentary paragneiss and Neoproterozoic to Permian intrusive rocks, updating earlier work by Lundgren (1967). From oldest to youngest, the metamorphic and igneous rocks in the Old Lyme quadrangle are (1) Neoproterozoic metasedimentary and metaigneous rocks of the Gander terrane, (2) Neoproterozoic rocks of the Avalon terrane, (3) Silurian and Devonian metasedimentary rocks, and (4) Pennsylvanian-Permian igneous rocks. This paper focuses on the Neoproterozoic basement gneisses of the Gander terrane in the core of the Lyme dome and the Permian intrusive rocks in the area. U-Pb ages were determined by analysis using the USGS/Stanford sensitive high resolution ion microprobe-reverse geometry (SHRIMP-RG) at Stanford University, Palo Alto, California. Ages of units described below are the weighted average of selected $^{206}Pb/^{238}U$ ages. Geochronology data are provided in tables 1 and 2, and summarized in figure 4. See the Appendix for a complete description of the geochronology procedures.

Neoproterozoic Rocks

The Gander terrane Neoproterozoic rocks in the Lyme dome include metasedimentary rocks of the Old Lyme Gneiss, and granodiorite and granite orthogneisses found on Becket Hill, Johnnycake Hill, and Lord Hill in the Old Lyme quadrangle (fig. 3; Walsh and others, 2006). Because previous names for metasedimentary rocks within the core of the Lyme dome are based on correlations with rocks that have type localities in the Avalon terrane in eastern and southeastern Connecticut, we use informal local names. Previous names for metasedimentary rocks in the Old Lyme quadrangle by Lundgren (1967) and Rodgers (1985) include the Plainfield Formation, the Mamacoke Formation, and the New London Gneiss. All of these rocks are now mapped as lithodemic units of the Old Lyme Gneiss (Walsh and others, 2006).

Old Lyme Gneiss

The Old Lyme Gneiss (new name) is applied to metasedimentary rocks with minor mafic metavolcanic rocks exposed in the core of the Lyme dome. Walsh and others (2006) mapped six different units within the dome, including biotite gneiss, garnetiferous biotite gneiss, sillimanite schist, quartzite, layered quartzite and schist, and amphibolite. Lundgren (1967) and Rodgers (1985) considered the sequence of Plainfield Formation, Mamacoke Formation, and New London Gneiss as metasedimen-

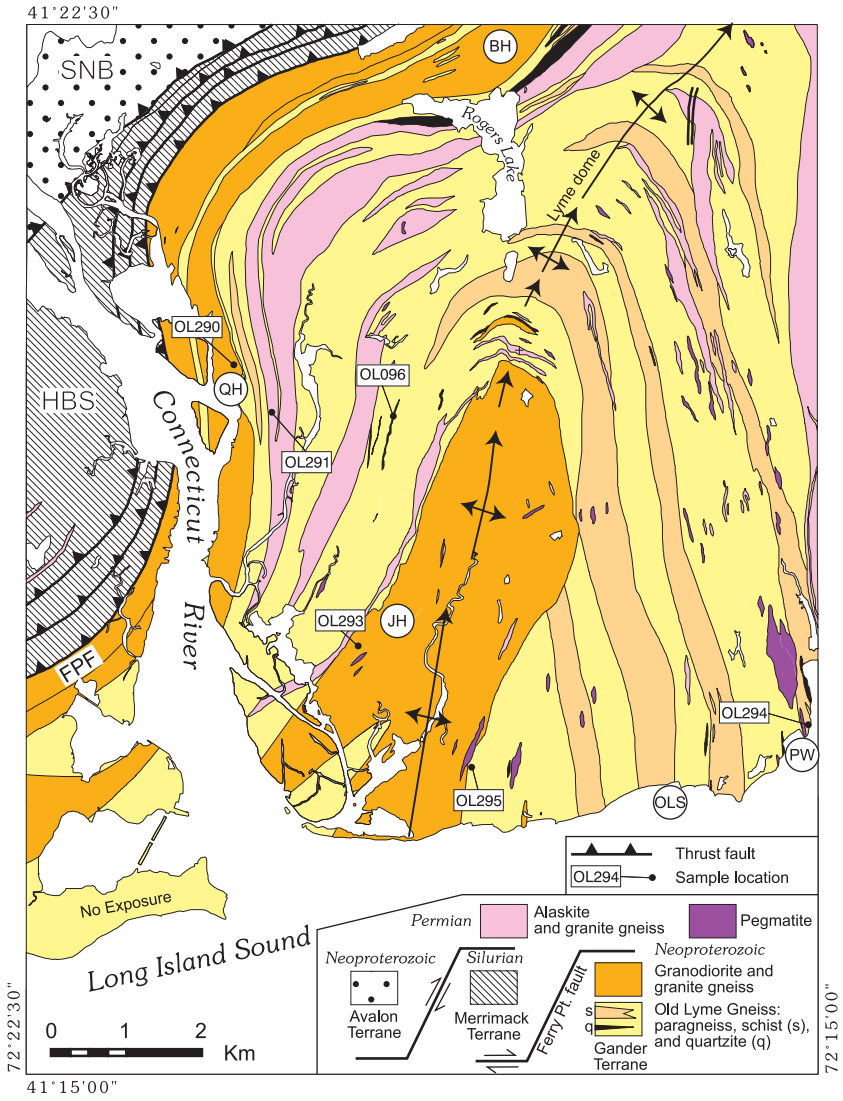

Fig. 3. Simplified geologic map of the Old Lyme quadrangle showing sample localities and axial trace of the Lyme dome; modified after Walsh and others (2006). Abbreviations: SNB – Selden Neck block, HBS – Hunts Brook slice, FPF – Ferry Point fault, BH – Becket Hill, JH – Johnnycake Hill, QH – Quarry Hill, OLS – Old Lyme Shores, and PW – Point O'Woods.

tary and metavolcanic rocks representing a continuous stratigraphic succession from oldest to youngest, despite the high degree of metamorphic and igneous overprinting experienced by the rocks. Our mapping agrees with the rock types identified by Lundgren (1967), but shows a different distribution for these rocks. Because sedimentary topping criteria are lacking in these rocks, and the contacts between the formations are occupied by meta-igneous rocks, the true stratigraphic succession cannot be determined from field observations. Type localities for all three formations occur outside the Lyme dome in the Avalon terrane, and these formation names are discontinued for use in the Lyme dome block. To assess the age, provenance, and metamorphic history of the metasedimentary and metavolcanic rocks in the Old Lyme Gneiss, we sampled a quartzite and an amphibolite from the Lyme dome.

TABLE 1

SHRIMP U-Th-Pb data for detrital zircon from quartzite in the Old Lyme Gneiss, south-central

sample[1]	measured $^{204}Pb/^{206}Pb$	measured $^{207}Pb/^{206}Pb$	% common ^{206}Pb	U (ppm)	Th/U	$^{206}Pb^{2}/^{238}U$(Ma)	err[3] (Ma)	$^{207}Pb^{2}/^{206}Pb$(Ma)	err[3] (Ma)	% disc.	$^{238}U/^{206}Pb$	err[3] (%)	$^{207}Pb^{2}/^{206}Pb$	err[3] (%)
OL096-1.1	0.000091	0.0842	0.17	118	0.5	1185.6	14.4	1267	48	6	4.93	1.2	0.0829	2.4
OL096-2.1	0.000116	0.0783	0.22	129	0.01	1132.4	15.5	1112	53	-2	5.21	1.4	0.0766	2.7
OL096-3.1	---	0.1149	0	129	0.93	1866.1	24.3	1878	32	1	2.98	1.3	0.1149	1.8
OL096-4.1	0.000078	0.1332	0.15	80	0.64	1976.1	7	2127	30	7	2.75	0.2	0.1321	1.7
OL096-5.1	---	0.0867	0	79	0.56	1272.2	21.5	1354	49	6	4.56	1.7	0.0867	2.5
OL096-6.1	---	0.1133	0	124	0.62	1783.3	15.6	1853	28	4	3.12	0.8	0.1133	1.5
OL096-7.1	---	0.0748	0	65	0.48	1022	13.3	1063	72	4	5.81	1.3	0.0748	3.6
OL096-8.1	---	0.0932	0	63	0.15	1510.2	18.6	1492	47	-1	3.79	1.2	0.0932	2.5
OL096-9.1	---	0.0752	0	103	0.26	999.7	13.6	1074	55	7	5.94	1.4	0.0752	2.8
OL096-10.1	0.000186	0.0866	0.35	94	0.33	1402	16.3	1292	77	-9	4.14	1.2	0.084	3.9
OL096-11.1	---	0.0782	0	47	0.39	1064	4.4	1151	74	8	5.55	0.2	0.0782	3.7
OL096-12.1	0.000713	0.1724	1.33	26	0.84	1328.9	36.2	2492	79	47	3.91	2.8	0.1634	4.7
OL096-13.1	---	0.0843	0	183	0.5	1107.3	10.5	1300	36	15	5.28	1	0.0843	1.9
OL096-14.1	---	0.0823	0	130	0.52	1246.3	3.1	1252	40	0	4.69	0.1	0.0823	2.1
OL096-15.1	0.000058	0.0947	0.11	195	0.46	1508.6	21.4	1507	29	0	3.79	1.4	0.0939	1.6
OL096-16.1	---	0.1237	0	109	0.48	1928.8	31.1	2011	28	4	2.84	1.6	0.1237	1.6
OL096-17.1	---	0.1268	0	193	0.72	1946.8	56.7	2054	19	5	2.81	2.8	0.1268	1.1
OL096-18.1	---	0.0824	0	78	0.49	1202.7	32.9	1255	52	4	4.86	2.8	0.0824	2.7
OL096-19.1	---	0.091	0	143	0.6	1213.6	3	1446	35	16	4.76	0.1	0.091	1.8
OL096-20.1	---	0.0882	0	82	0.92	1225.8	3.9	1387	48	12	4.73	0.1	0.0882	2.5
OL096-21.1	-0.000223	0.0811	-0.42	71	0.33	1187.8	25.4	1297	80	8	4.91	2.2	0.0842	4.1
OL096-22.1	---	0.0824	0	151	0.43	1236.3	5.6	1256	37	2	4.73	0.4	0.0824	1.9
OL096-23.1	-0.000016	0.0932	-0.03	250	0.32	1498.2	3.8	1497	24	0	3.82	0.2	0.0934	1.3
OL096-24.1	0.000028	0.0928	0.05	302	0.23	1462.7	33.3	1476	23	1	3.92	2.3	0.0924	1.2
OL096-25.1	0.000062	0.0832	0.12	145	0.45	1317.6	34.4	1253	84	-5	4.43	2.6	0.0823	4.3
OL096-26.1	---	0.0745	0	77	1.27	946.7	18.5	1056	71	10	6.29	2	0.0745	3.5
OL096-27.1	---	0.1152	0	99	0.84	1825.7	71.2	1882	29	3	3.04	3.9	0.1152	1.6
OL096-28.1	---	0.0913	0	261	0.5	1477.2	33.2	1453	29	-2	3.89	2.3	0.0913	1.5
OL096-29.1	---	0.0804	0	70	0.58	1227.2	14.5	1207	58	-2	4.77	1.2	0.0804	2.9
OL096-30.1	---	0.1059	0	87	0.67	1710	46.4	1730	34	1	3.29	2.7	0.1059	1.9
OL096-31.1	0.000064	0.079	0.12	160	0.33	1139.1	2.6	1150	41	1	5.17	0.2	0.0781	2
OL096-32.1	0.000132	0.0909	0.25	127	0.27	1419.2	7.9	1405	42	-1	4.06	0.5	0.0891	2.2
OL096-33.1	0.000094	0.0909	0.18	185	0.24	1401.6	16.7	1418	33	1	4.11	1.2	0.0896	1.7

TABLE 1

(continued)

sample[1]	measured $^{204}Pb/^{206}Pb$	measured $^{207}Pb/^{206}Pb$	% common ^{206}Pb	U (ppm)	Th/U	$^{206}Pb^{2}/^{238}U$(Ma)	err[3] (Ma)	$^{207}Pb^{2}/^{206}Pb$(Ma)	err[3] (Ma)	% disc.	$^{238}U/^{206}Pb$	err[3] (%)	$^{207}Pb^{2}/^{206}Pb$	err[3] (%)
OL096-34.1	---	0.0808	0	140	0.26	1231.1	15.6	1216	40	-1	4.76	1.3	0.0808	2
OL096-35.1	---	0.0862	0	265	0.39	1339.6	14.9	1342	26	0	4.33	1.1	0.0862	1.3
OL096-36.1	---	0.0876	0	251	0.91	1207.6	28.5	1373	28	12	4.81	2.4	0.0876	1.4
OL096-37.1	---	0.0695	0	147	0.49	925.7	22.4	915	50	-1	6.48	2.5	0.0695	2.4
OL096-38.1	---	0.072	0	102	0.34	1041.8	11.6	987	54	-6	5.72	1.1	0.072	2.7
OL096-39.1	0.000323	0.0775	0.6	37	0.52	1369.1	31.8	1012	110	-35	4.31	2.4	0.0729	5.4
OL096-40.1	---	0.1275	0	267	0.37	2083	13.8	2063	15	-1	2.63	0.6	0.1275	0.8
OL096-41.1	0.000038	0.1146	0.07	158	0.56	1944.1	19	1865	23	-4	2.86	0.9	0.1141	1.3
OL096-42.1	---	0.0828	0	291	0.28	1185.2	27.2	1265	27	6	4.93	2.4	0.0828	1.4
OL096-43.1	0.00015	0.0798	0.28	62	0.26	1235.6	5.7	1138	68	-9	4.76	0.4	0.0777	3.4
OL096-44.1	---	0.0787	0	283	0.24	893.8	14.4	1166	37	23	6.64	1.6	0.0787	1.9
OL096-45.1	0.000052	0.0812	0.1	172	0.6	1205.4	7.3	1209	36	0	4.86	0.6	0.0805	1.8
OL096-46.1	0.000084	0.1105	0.16	98	0.47	1755	48.7	1789	32	2	3.19	2.8	0.1094	1.8
OL096-47.1	---	0.0832	0	285	0.5	1201.6	21.1	1274	28	6	4.86	1.8	0.0832	1.4
OL096-48.1	---	0.0827	0	302	0.33	1211.7	24.3	1262	26	4	4.82	2.1	0.0827	1.3
OL096-49.1	---	0.0816	0	303	0.39	1234.9	43.2	1235	34	0	4.74	3.6	0.0816	1.7
OL096-50.1	---	0.0753	0	276	0.77	955.9	28.2	1076	33	11	6.22	3	0.0753	1.6

[1] Analyzed on the USGS/Stanford SHRIMP-RG in 12/02. Analyses in italics are discordant and not used in Relative Probability plot.

[2] Corrected for common Pb. $^{206}Pb/^{238}U$ ages corrected for common Pb using the ^{207}Pb-correction method; $^{207}Pb/^{206}Pb$ and $^{238}U/^{206}Pb$ corrected for common Pb using the ^{204}Pb-correction method. Decay constants from Steiger and Jäger (1977).

[3] 1-sigma error.

Description of sample location (latitude and longitude in NAD27 datum):
OL096 Old Lyme Gneiss quartzite (41° 19′ 41″ N, 72° 19′ 01″ W)
Sampled from an outcrop in the woods east of Hillwood Drive, Old Lyme, CT.

TABLE 2

SHRIMP U-Th-Pb data for zircon and monazite from igneous rocks of the Lyme dome, south-central Connecticut. Latitutde and longitude in NAD27 datum.

sample[1] (location)	measured $^{204}Pb/^{206}Pb$	measured $^{207}Pb/^{206}Pb$	common ^{206}Pb	% U (ppm)	Th/U	$^{206}Pb^{2}/^{238}U$(Ma)	err[3] (Ma)	$^{238}U^{4}/^{206}Pb$	err[3] (%)	$^{207}Pb^{4}/^{206}Pb$	err[3] (%)	$^{207}Pb^{2,5}/^{206}Pb$(Ma)	err[3] (Ma)
OL295 Old Lyme Gneiss amphibolite (41° 17′ 11″ N, 72° 18′ 08″ W)													
Sampled from a roadcut on the north side of Route 156, Old Lyme, CT.													
OL295-1.1cdk	0.010771	0.1022	6.29	4	0.05	273.4	17.9	21.63	6.1	.1022	18.6		
OL295-2.1cdk	0.010949	0.0926	5.04	7	0.01	294.4	11.5	20.32	3.6	.0926	13.9		
OL295-3.1cdk	0.004130	0.0809	3.58	7	0.02	293.7	11.2	20.68	3.6	.0809	14.4		
OL295-4.1cdk	-0.022027	0.0771	3.15	2	0.01	276.2	17.6	22.12	6.0	.0771	25.3		
OL295-5.1cdk	0.003640	0.0595	0.93	9	0.01	286.6	8.8	21.79	3.0	.0595	11.1		
OL295-6.1x	0.000984	0.0627	0.34	8	0.00	601.3	19.8	10.19	3.3	.0627	8.2		
OL295-6.2x	-0.002117	0.0734	1.76	8	0.00	567.4	15.1	10.68	2.6	.0734	7.7		
OL295-7.1cdk	-0.002357	0.0457	-0.78	4	0.03	283.6	12.7	22.41	4.3	.0457	26.0		
OL295-8.1cdk	0.003339	0.0679	1.99	5	0.02	284.6	11.5	21.71	3.9	.0679	14.9		
OL295-9.1cdk	-0.000933	0.0655	1.27	7	0.16	420.8	13.2	14.64	3.1	.0655	11.0		
OL295-10.1clt	-0.005565	0.0549	0.41	10	0.01	269.9	8.3	23.29	3.0	.0549	12.6		
OL295-11.1cdk	0.000000	0.0636	1.43	10	0.01	289.2	8.8	21.48	3.0	.0636	10.7		
OL295-12.1clt	0.001561	0.0539	0.30	10	0.01	263.0	7.8	23.94	2.9	.0539	12.3		
OL295-13.1clt	0.001713	0.0562	0.55	15	0.03	273.2	7.1	22.97	2.5	.0562	10.4		
OL295-14.1cdk	-0.000680	0.0578	0.73	9	0.03	281.6	8.9	22.23	3.1	.0578	12.4		
OL295-15.1rlt	0.003108	0.0561	0.58	11	0.05	259.5	7.8	24.20	2.9	.0561	12.1		
OL295-16.1cdk	0.003866	0.0566	0.59	11	0.06	280.1	8.0	22.39	2.8	.0566	11.8		
OL295-17.1clt	0.000000	0.0574	0.70	13	0.01	277.3	7.5	22.59	2.6	.0574	9.5		
OL295-18.1rlt	-0.004971	0.0777	3.23	6	0.01	275.1	10.1	22.20	3.5	.0777	12.0		
OL295-19.1cdk	0.005387	0.0595	0.95	10	0.02	280.0	8.2	22.31	2.9	.0595	10.5		
OL290 granite gneiss at Becket Hill (41° 20′ 06″ N, 72° 22′ 30″ W)													
Sampled from an outcrop on the north side of Quarry Hill off Binney Road, Old Lyme, CT.													
OL290-1.1c	0.000095	0.0613	0.17	265	1.18	599.9	4.8	10.25	0.8	.0599	2.0	601	44
OL290-2.1c	---	0.0602	0.00	220	0.85	611.4	5.1	10.05	0.8	.0602	1.9	610	41
OL290-3.1c	---	0.0601	-0.06	1516	0.48	623.3	4.0	9.86	0.7	.0601	0.8	605	17
OL290-4.1c	0.000362	0.0612	0.21	169	1.05	584.3	5.3	10.59	1.0	.0559	4.4	449	97
OL290-5.1c	0.000064	0.0597	0.03	568	0.61	586.3	3.9	10.51	0.7	.0588	1.4	561	31
OL290-6.1c	---	0.0593	-0.06	194	0.78	595.7	5.1	10.34	0.9	.0593	2.0	579	43
OL290-7.1c	0.000044	0.0592	0.11	539	0.48	540.8	3.6	11.42	0.7	.0585	1.4	549	31
OL290-8.1c	---	0.0597	0.01	127	0.89	587.7	6.2	10.48	1.1	.0597	2.6	592	56

TABLE 2
(continued)

sample[1] (location)	measured $^{204}Pb/^{206}Pb$	measured $^{207}Pb/^{206}Pb$	common ^{206}Pb	% U (ppm)	Th/U	$^{206}Pb^{2}/^{238}U$(Ma)	err[3] (Ma)	$^{238}U^{4}/^{206}Pb$	err[3] (%)	$^{207}Pb^{4}/^{206}Pb$	err[3] (%)	$^{207}Pb^{2,5}/^{206}Pb$(Ma)	err[3] (Ma)
OL290-9.1c	---	0.0588	0.11	245	0.58	525.7	4.5	11.76	0.9	.0588	2.1	559	45
OL290-10.1c	---	0.0609	0.13	415	0.53	597.4	4.2	10.28	0.7	.0609	1.4	636	30
OL290-11.1c	---	0.0609	0.08	342	0.85	612.4	4.6	10.03	0.8	.0609	1.6	635	34
OL290-12.1c	---	0.0599	-0.04	227	1.21	614.0	5.3	10.01	0.9	.0599	1.9	602	42
OL290-13.1c	---	0.0615	0.17	361	0.46	607.4	4.6	10.10	0.8	.0615	1.6	656	34
OL290-14.1c	---	0.0596	0.24	280	0.93	516.9	4.7	11.95	0.9	.0596	2.2	589	48
OL290-15.1c	---	0.0608	0.08	111	0.98	606.7	7.4	10.12	1.2	.0608	3.1	631	68
OL290-16.1c	---	0.0612	0.09	459	0.53	621.0	4.5	9.88	0.7	.0612	1.5	647	31
OL290-16.2r	---	0.0504	-0.25	1190	0.02	300.4	1.9	21.02	0.6	.0504	2.0		
OL290-17.1c	-0.000048	0.0609	0.08	455	0.75	613.0	4.3	10.01	0.7	.0616	1.6	661	34
OL290-18.1r	---	0.0520	0.00	1497	0.04	286.7	1.8	21.99	0.6	.0520	1.3		
OL293 granodiorite gneiss at Johnnycake Hill (41° 18′ 03″ N, 72° 19′ 22″ W)													
Sampled from a railroad cut on the north side of the Penn Central railroad near Black Hall, Old Lyme, CT.													
OL293-1.1c	---	0.0607	0.0595	274	0.82	611.3	9.1	10.05	1.5	.0607	1.8	629	39
OL293-2.1c	---	0.0638	0.4400	155	0.82	610.5	9.6	10.02	1.6	.0638	2.4	735	51
OL293-3.1c	---	0.0587	-0.2839	187	0.68	640.7	10.0	9.60	1.6	.0587	2.2	557	48
OL293-4.1r	0.000057	0.0535	0.1570	1805	0.03	295.5	3.9	21.31	1.4	.0527	1.4	314	32
OL293-5.1r	---	0.0606	0.8983	122	0.13	345.1	6.2	18.02	1.8	.0606	4.3	626	93
OL293-6.1c	---	0.0602	0.0305	293	0.72	600.9	8.7	10.23	1.5	.0602	2.1	610	45
OL293-7.1r	---	0.0578	0.5607	275	0.12	341.1	5.3	18.30	1.6	.0578	2.7	522	59
OL293-8.1c	---	0.0600	-0.0474	260	0.58	617.5	9.0	9.95	1.5	.0600	1.9	604	42
OL293-9.1c	---	0.0617	0.2691	142	0.83	586.6	9.4	10.47	1.6	.0617	2.6	665	55
OL293-10.1r	0.000157	0.0556	0.3462	898	0.04	321.5	4.8	19.54	1.5	.0533	2.5	342	56
OL293-11.1c	---	0.0600	-0.0041	290	1.20	603.6	8.7	10.19	1.5	.0600	1.9	602	42
OL293-12.1c	---	0.0602	-0.0908	259	0.75	635.5	9.2	9.66	1.5	.0602	1.9	609	40
OL293-13.1c	---	0.0603	-0.0168	382	1.10	617.7	8.7	9.95	1.4	.0603	1.6	613	35
OL293-14.1c	---	0.0618	0.0673	101	0.64	646.9	11.0	9.47	1.7	.0618	3.0	666	64
OL293-15.1c	---	0.0596	-0.1215	683	0.32	626.0	8.5	9.82	1.4	.0596	1.4	590	29
OL293-16.1c	---	0.0599	-0.1033	236	0.74	631.7	9.6	9.72	1.6	.0599	2.0	601	43
OL293-18.1c	---	0.0590	-0.1445	327	0.85	611.9	8.7	10.06	1.5	.0590	1.7	569	38
OL293-19.1c	---	0.0599	-0.0370	187	0.60	611.6	9.4	10.05	1.6	.0599	2.3	601	50
OL293-20.1c	---	0.0616	0.1753	150	0.77	608.7	9.7	10.08	1.6	.0616	2.6	659	56
OL293-21.1c	---	0.0600	-0.0959	409	0.92	632.4	8.8	9.71	1.4	.0600	1.5	604	32
OL293-22.1c	---	0.0608	0.0491	341	0.71	616.7	8.7	9.96	1.4	.0608	1.7	631	36

TABLE 2
(continued)

sample[1] (location)	measured $^{204}Pb/^{206}Pb$	measured $^{207}Pb/^{206}Pb$	common ^{206}Pb	% U (ppm)	Th/U	$^{206}Pb^{2}/^{238}U$(Ma)	err[3] (Ma)	$^{238}U^{4}/^{206}Pb$	err[3] (%)	$^{207}Pb^{4}/^{206}Pb$	err[3] (%)	$^{207}Pb^{2,5}/^{206}Pb$(Ma)	err[3] (Ma)
OL291 alaskite gneiss (41° 19′ 44″ N, 72° 20′ 10″ W)													
Sampled from a roadcut on Talcott Farm Road, Old Lyme, CT.													
OL291-1.1r	---	0.0518	-0.07	5361	0.05	*299.5*	3.9	21.04	1.3	.0518	0.7	276	15
OL291-2.1c	---	0.0525	0.05	4717	0.06	289.1	3.8	21.79	1.3	.0525	0.7	307	16
OL291-3.1r	---	0.0510	-0.09	3067	0.05	276.2	3.7	22.86	1.4	.0510	1.0	242	22
OL291-4.1r	0.000028	0.0521	0.00	5076	0.08	*288.0*	3.9	21.90	1.4	.0517	0.8	271	18
OL291-5.1c	0.000012	0.0522	-0.01	5435	0.05	*296.9*	3.9	21.22	1.3	.0520	0.7	286	16
OL291-6.1c	---	0.0519	-0.01	4446	0.05	286.6	3.8	22.00	1.3	.0519	0.8	282	17
OL291-7.1r	0.000070	0.0531	0.16	4080	0.06	278.4	3.7	22.65	1.3	.0521	1.1	289	26
OL291-8.1x	---	0.0600	-0.07	594	0.63	625.3	8.5	9.82	1.4	.0600	1.3	605	27
OL291-9.1r	0.000525	0.0597	0.97	4035	0.05	282.8	3.7	22.30	1.3	.0521	2.0	288	47
OL291-10.1x	---	0.0604	0.03	700	0.64	608.4	8.2	10.10	1.4	.0604	1.2	617	26
OL291-11.1c	---	0.0527	0.06	3038	0.05	291.8	3.8	21.59	1.3	.0527	0.9	314	20
OL291-13.1c	---	0.0524	0.01	6062	0.05	*297.6*	3.9	21.16	1.3	.0524	0.7	301	15
OL291-14.1x	---	0.0600	-0.05	1725	0.36	617.7	8.3	9.95	1.4	.0600	0.8	602	17
OL291-15.1c	0.000017	0.0527	0.09	3346	0.05	286.0	3.8	22.03	1.3	.0525	1.2	306	27
OL291-16.1c	---	0.0526	0.05	3551	0.05	294.6	3.9	21.37	1.3	.0526	0.8	312	18
OL291-17.1r	0.000025	0.0521	0.03	2342	0.07	276.9	3.7	22.79	1.3	.0517	1.1	273	25
OL291-18.1c	0.000015	0.0523	0.02	5110	0.06	*294.6*	*3.9*	21.39	1.3	.0521	0.7	291	16
OL294B granite pegmatite (41° 17′ 30″ N, 72° 15′ 06″ W)													
Sampled from an outcrop on Long Island Sound at Point O' Woods, Old Lyme, CT.													
OL294B-1.2x	---	0.0886	0.24	62	0.78	1351.9	26.4	4.28	2.0	.0886	2.5	1396	47
OL294B-2.1m	0.000100	0.0537	0.22	1669	0.08	285.5	4.1	22.08	1.4	.0523	2.0		
OL294B-3.1m	---	0.0514	-0.06	524	0.10	281.5	4.4	22.41	1.6	.0514	2.6		
OL294B-4.1m	---	0.0538	0.23	373	0.18	283.2	4.6	22.21	1.6	.0538	2.8		
OL294B-5.1c	0.000453	0.0592	0.93	1975	0.12	272.7	3.9	23.12	1.4	.0525	3.6		
OL294B-6.1	0.000081	0.0520	-0.03	677	0.12	296.0	4.4	21.32	1.5	.0508	2.9		
OL294B-7.1c	---	0.0531	0.14	673	0.09	285.2	4.3	22.07	1.5	.0531	2.2		
OL294B-8.1m	---	0.0528	0.08	1296	0.08	290.8	4.2	21.66	1.5	.0528	1.6		
OL294B-10.1m	---	0.0519	-0.05	472	0.09	299.0	4.6	21.08	1.6	.0519	2.5		
OL294B-11.1c	---	0.0529	0.09	696	0.07	291.2	4.4	21.62	1.5	.0529	2.2		
OL294B-12.1c	---	0.0521	0.02	692	0.13	283.1	4.3	22.27	1.5	.0521	2.2		
OL294B-13.1c	---	0.0519	-0.03	498	0.10	290.1	4.5	21.73	1.6	.0519	2.7		
OL294B-14.1c	---	0.0520	-0.01	609	0.12	287.3	4.4	21.95	1.5	.0520	2.3		

TABLE 2
(continued)

sample[1] (location)	measured $^{204}Pb/^{206}Pb$	measured $^{207}Pb/^{206}Pb$	common ^{206}Pb	% U (ppm)	Th/U	$^{206}Pb^{2}/^{238}U$(Ma)	err[3] (Ma)	$^{238}U^{4}/^{206}Pb$	err[3] (%)	$^{207}Pb^{4}/^{206}Pb$	err[3] (%)	$^{207}Pb^{2,5}/^{206}Pb$(Ma)	err[3] (Ma)
OL294Bmz-1.1csz	0.000557	0.0551	0.38	1215	57.2	291.2	2.7	21.78	0.9	.0469	3.2		
OL294Bmz-2.1coz	0.000368	0.0548	0.34	2202	24.2	287.2	1.9	22.02	0.7	.0493	1.8		
OL294Bmz-3.1cuz	0.000485	0.0538	0.22	2547	34.6	288.7	1.9	21.98	0.7	.0467	2.0		
OL294Bmz-4.1coz	0.000648	0.0548	0.34	1693	53.4	287.3	2.0	22.13	0.7	.0452	3.0		
OL294Bmz-5.1cuz	0.001428	0.0592	0.89	607	114.0	288.9	2.5	22.20	0.9	.0379	8.0		
OL294Bmz-6.1csz	0.000907	0.0549	0.36	1252	55.8	286.2	2.1	22.32	0.8	.0415	4.4		
OL294Bmz-7.1coz	0.001315	0.0560	0.61	2881	78.8	245.1	2.3	26.28	1.1	.0363	12.2		
OL294Bmz-8.1coz	0.000601	0.0542	0.28	2161	47.2	283.1	1.9	22.46	0.7	.0453	2.5		
OL294Bmz-9.1csp	0.000586	0.0537	0.25	1921	45.4	274.1	1.9	23.21	0.7	.0451	2.8		
OL294Bmz-10.1csp	0.000853	0.0557	0.49	1266	66.4	276.2	2.1	23.09	0.8	.0431	3.8		
OL294Bmz-11.1coz	0.000699	0.0543	0.37	1665	43.5	258.5	2.1	24.67	0.8	.0440	3.0		
OL294Bmz-12.1cuz	0.000621	0.0547	0.42	2263	47.2	254.6	1.7	25.00	0.7	.0455	2.5		
OL294Bmz-13.1csp	0.000233	0.0525	0.13	4292	14.8	259.2	1.6	24.44	0.6	.0491	1.1		
OL294Bmz-14.1cuz	0.000968	0.0557	0.53	1206	70.6	264.2	1.9	24.20	0.7	.0414	4.0		
OL294Bmz-15.1cuz	0.001048	0.0545	0.38	1246	72.5	260.1	1.9	24.66	0.8	.0389	4.5		
OL294Bmz-16.1ruz	0.001166	0.0567	0.63	903	84.7	269.4	2.0	23.79	0.8	.0393	5.2		
OL294Bmz-16.2csp	0.001075	0.0563	0.58	1138	83.3	270.3	2.1	23.69	0.9	.0403	6.4		
OL294A Westerly Granite (41° 17′ 30″ N, 72° 15′ 06″ W)													
Sampled from an outcrop on Long Island Sound at Point O' Woods, Old Lyme, CT.													
OL294A-1.1m	---	0.0536	0.18	398	0.16	294.9	4.3	21.33	1.5	.0536	2.1		
OL294A-2.1m	---	0.0525	0.09	405	0.31	276.6	4.0	22.79	1.5	.0525	2.1		
OL294A-3.1c	0.000097	0.0524	0.07	511	0.29	279.5	4.0	22.59	1.4	.0510	2.3		
OL294A-4.1m	---	0.0510	-0.14	525	0.19	288.3	4.1	21.89	1.4	.0510	1.9		
OL294A-5.1m	---	0.0528	0.11	374	0.01	281.8	4.3	22.35	1.6	.0528	2.4		
OL294A-6.1r	0.000624	0.0592	0.93	1210	0.19	272.9	3.8	23.18	1.4	.0500	4.4		
OL294A-1.2c	0.000062	0.0897	1.33	230	0.38	1160.5	16.3	5.01	1.5	.0889	1.2	1401	23
OL294A-7.1r	0.007341	0.1745	15.03	1327	0.29	347.4	7.7	17.70	2.0	.0692	25.6		
OL294A-8.1c	---	0.0508	-0.07	169	0.91	258.7	4.3	24.43	1.7	.0508	3.6		
OL294A-9.1r	0.000663	0.0619	1.32	1194	0.17	254.5	3.5	24.80	1.4	.0521	4.9		
OL294A-10.1r	0.000265	0.0518	0.04	235	0.91	260.5	4.1	24.36	1.6	.0479	5.0		
OL294A-11.1r	0.001603	0.0787	3.32	400	0.24	288.0	4.5	21.80	1.8	.0553	14.7		
OL294A-12.1c	---	0.0536	0.24	367	0.41	272.5	4.1	23.10	1.5	.0536	2.4		
OL294A-13.1r	0.000158	0.1847	14.99	657	0.26	665.2	11.1	7.84	1.4	.1828	3.6	2678	59

TABLE 2
(continued)

sample[1] (location)	measured $^{204}Pb/^{206}Pb$	measured $^{207}Pb/^{206}Pb$	common ^{206}Pb	% U (ppm)	Th/U	$^{206}Pb^{2}/^{238}U$(Ma)	err[3] (Ma)	$^{238}U^{4}/^{206}Pb$	err[3] (%)	$^{207}Pb^{4}/^{206}Pb$	err[3] (%)	$^{207}Pb^{2,5}/^{206}Pb$(Ma)	err[3] (Ma)
OL294A-14.1r	0.001233	0.0635	1.47	1544	0.04	272.6	3.8	23.34	1.5	.0453	7.9		
OL294A-15.1r	0.000604	0.0631	1.40	669	0.15	280.0	4.1	22.46	1.5	.0543	5.6		
OL294A-16.1r	---	0.0540	0.30	211	0.04	269.2	4.4	23.38	1.6	.0540	3.2		
OL294A-17.1c	---	0.0496	-0.26	101	1.13	273.0	5.1	23.18	1.9	.0496	4.8		
OL294A-18.1c	0.000251	0.0505	-0.13	228	0.11	264.1	4.2	24.05	1.6	.0468	4.8		
OL294Amz-1.1cuz	0.001555	0.0530	0.18	710	121.8	264.1	2.1	24.57	0.9	.0295	10.2		
OL294Amz-2.1cuz	0.000365	0.0544	0.34	588	71.2	270.9	3.1	23.38	1.2	.0490	4.1		
OL294Amz-3.1cuz	0.000942	0.0531	0.19	693	79.7	268.8	2.2	23.86	0.9	.0391	6.2		
OL294Amz-3.2ruz	0.000309	0.0529	0.19	2860	17.8	260.0	1.7	24.39	0.7	.0484	1.5		
OL294Amz-4.1cuz	0.000920	0.0540	0.33	850	123.2	257.4	2.0	24.89	0.8	.0403	5.8		
OL294Amz-5.1cuz	0.000971	0.0546	0.40	983	119.9	258.5	2.0	24.79	0.8	.0401	5.6		
OL294Amz-5.2ruz	0.000774	0.0531	0.18	1249	46.4	273.0	1.9	23.41	0.7	.0416	3.2		
OL294Amz-6.1roz	0.000414	0.0522	0.11	2041	36.9	254.4	1.8	25.00	0.7	.0461	2.3		
OL294Amz-7.1ruz	0.000887	0.0551	0.44	475	96.6	264.3	2.4	24.18	1.0	.0419	6.6		
OL294Amz-8.1ruz	0.001012	0.0543	0.36	687	97.5	259.1	2.1	24.75	0.9	.0393	6.4		
OL294Amz-9.1roz	0.000951	0.0537	0.28	757	118.4	260.9	2.1	24.57	0.9	.0395	5.7		
OL294Amz-10.1cuz	0.000375	0.0534	0.22	607	71.4	269.7	2.2	23.51	0.9	.0478	3.8		
OL294Amz-11.1roz	0.000655	0.0540	0.33	720	79.6	257.0	2.1	24.81	0.8	.0443	4.2		
OL294Amz-12.1cuz	0.001089	0.0561	0.58	444	91.1	262.9	2.4	24.37	1.0	.0399	8.8		
OL294Amz-13.1roz	0.000567	0.0531	0.21	1220	49.8	258.1	1.9	24.69	0.8	.0447	3.0		

TABLE 2

(continued)

sample[1] (location)	measured $^{204}Pb/^{206}Pb$	measured $^{207}Pb/^{206}Pb$	common ^{206}Pb	% U (ppm)	Th/U	$^{206}Pb^{2}/^{238}U$(Ma)	err[3] (Ma)	$^{238}U^{4}/^{206}Pb$	err[3] (%)	$^{207}Pb^{4}/^{206}Pb$	err[3] (%)	$^{207}Pb^{2,5}/^{206}Pb$(Ma)	err[3] (Ma)
PEC-702 Joshua Rock Granite Gneiss (Zartman and others, 1988; 41° 22' 33" N, 72° 08' 42" W)													
PEC-1.1c	0.001355	0.0697	2.13	278	0.13	307.9	4.4	20.51	1.6	.0497	12.3		
PEC-2.1c	0.000218	0.0516	-0.07	356	0.23	292.1	4.2	21.67	1.5	.0483	6.1		
PEC-3.1c	---	0.0499	-0.26	415	0.22	284.0	4.0	22.26	1.4	.0499	2.3		
PEC-4.1c	---	0.0519	-0.02	396	0.26	288.8	4.0	21.83	1.4	.0519	2.2		
PEC-5.1c	---	0.0538	0.27	119	0.47	270.0	4.8	23.32	1.8	.0538	3.9		
PEC-6.1c	-0.000068	0.0515	-0.05	324	0.12	283.2	4.1	22.25	1.4	.0525	3.5		
PEC-7.1c	---	0.0521	0.02	89	0.48	282.4	5.7	22.33	2.0	.0521	4.8		
PEC-8.1c	0.000153	0.0525	0.07	340	0.24	281.1	4.0	22.48	1.4	.0502	3.4		
PEC-9.1c	0.000069	0.0516	-0.02	366	0.34	275.5	3.9	22.94	1.4	.0506	3.1		
PEC-10.1c	---	0.0526	0.10	299	0.30	279.5	4.1	22.55	1.5	.0526	2.8		
PEC-11.1c	---	0.0554	0.44	127	0.84	280.8	4.9	22.36	1.8	.0554	3.7		
PEC-12.1c	---	0.0508	-0.14	536	0.46	282.8	3.8	22.33	1.3	.0508	2.1		
PEC-13.1c	---	0.0540	0.23	430	0.24	289.5	4.0	21.72	1.4	.0540	2.6		
PEC-15.1c	---	0.0527	0.10	366	0.25	281.2	3.9	22.41	1.4	.0527	2.3		
PEC-16.1c	0.000274	0.0528	0.09	307	0.18	285.5	4.1	22.18	1.5	.0487	5.4		
PEC-17.1fr	0.003322	0.0950	5.35	351	0.12	287.9	4.1	22.06	1.7	.0459	18.0		

[1] Sample names with suffix "mz" are monazite; all other samples are zircon. All samples analyzed on the USGS/Stanford ion microprobe (SHRIMP-RG). Abbreviations: c (core), m (mantle), r (rim), fr (framboidal), dk (dark), lt (light), x (xenocryst).

[2] $^{206}Pb/^{238}U$ ages corrected for common Pb using the ^{207}Pb-correction method; $^{207}Pb/^{206}Pb$ ages corrected for common Pb using the ^{204}Pb-correction method. Decay constants from Steiger and Jäger (1977). For sample OL-291, $^{206}Pb/^{238}U$ ages shown in italics not used.

[3] 1-sigma errors.

[4] Radiogenic ratios, corrected for common Pb using the ^{204}Pb-correction method, based on the Stacey and Kramers (1975) model.

[5] Listed only for ages >1.0 Ga.

A

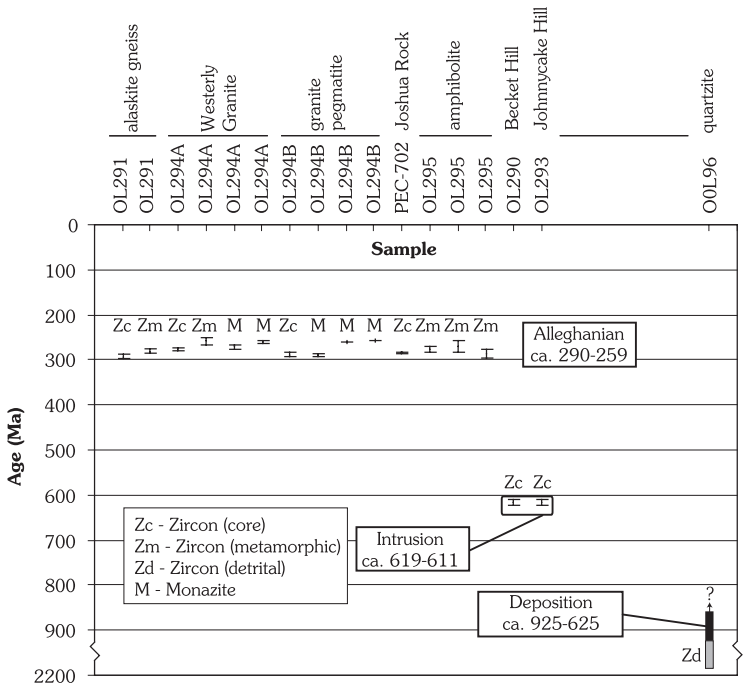

B

Sample	Rock		Ages (Ma)
Permian Rocks			
OL295	Old Lyme Gneiss amphibolite - metamorphic zircons		270 ± 7 and 285 ± 6
OL294A	Westerly Granite dike	- zircon cores	275 ± 4
		- metamorphic zircons	259 ± 4
		- monazite	271 ± 3 and 259 ± 2
PEC-702	Joshua Rock Granite Gneiss - zircon cores		284 ± 3
OL294B	Granite pegmatite	- zircon cores	288 ± 4
		- monazite	287 ± 2, ~263 and ~260
OL291	Alaskite gneiss - cores (c) and rims (r)		290 ± 4 (c) and 279 ± 4 (r)
Neoproterozoic Rocks			
OL290	Granite gneiss at Becket Hill - zircon cores		611 ± 8
OL293	Granodiorite gneiss at Johnnycake Hill - zircon cores		619 ± 7
OL096	Old Lyme Gneiss quartzite - detrital zircons		ca. 925 - 2127 Peaks at ca. 980, 1215, 1460, 1830, and 2060

Fig. 4. Summary diagram (A) and table (B) of U-Pb SHRIMP ages for rocks in the Lyme dome area, Connecticut. Sample PEC-702 is from Zartman and others (1988).

Quartzite (sample OL096) was collected from a 2-m-thick layer on the west flank of the Lyme dome (fig. 3). The rock consists of approximately 90 percent quartz, 8 percent interstitial K-feldspar and plagioclase, 2 percent biotite, and trace amounts of muscovite, clinozoisite, sphene, and zircon. The sampled quartzite is interlayered within the biotite gneiss unit and was traced for over 800 meters. Mapping indicates that the biotite gneiss unit is intruded by granodiorite gneiss in the core of the Lyme dome (fig. 3).

Detrital zircons are rounded, pitted, and frosted. As shown by CL, oscillatory zoning is truncated because the zircon grains were mechanically abraded during

sedimentation (fig. 5A). The zircons range in age from ca. 2127 to 925 Ma (table 1); seven discordant analyses (fig. 5B) are excluded from the Relative Probability plot (fig. 5C). The largest age group is ca. 1250 to 1130 Ma; subsidiary groups are ca. 1060 to 935, 1500 to 1300, 1900 to 1700, and 2125 to 2000 Ma. Similar age distributions for detrital zircons were found by Barr and others (2003) in Neoproterozoic metasedimentary rocks of peri-Gondwanan terranes in New Brunswick and Nova Scotia, Canada. The age of the quartzite is bracketed by the youngest detrital zircons at ca. 925 Ma and the oldest intrusive rocks that cut the Old Lyme Gneiss rocks at ca. 620 Ma.

Amphibolite (sample OL295) was collected from a 3- to 4-m-thick biotite-quartz-plagioclase hornblende gneiss that occurs as a disarticulated boudin within the biotite gneiss on the east flank of the Lyme dome (fig. 3). The amphibolite is interpreted as a metamorphosed basaltic rock (Walsh and others, 2006).

Zircons from sample OL295 are equant, discoidal, and colorless. In CL, they show faint oscillatory zoning, patchwork zoning, or are unzoned. Many grains have visible (in CL) cores and thin overgrowths (fig. 5D). These characteristics are typical of zircons of metamorphic origin (Hoskin and Schaltegger, 2003; Aleinikoff and others, 2006). These zircons formed during high grade metamorphism of the basalt protolith, when Zr was released from igneous pyroxene during reaction to form amphibole.

SHRIMP analyses of these zircons indicate that they have very low U contents (4-15 ppm) and very low Th/U (0.01 – 0.16, mostly <0.05) (table 2); the low Th/U values are typical of formation during high grade metamorphism. $^{206}Pb/^{238}U$ ages for 17 analyses range from ca. 294 to 260 Ma. Because these grains contain such low concentrations of U, the uncertainties of the individual ages are rather large (see overlapping error ellipses in fig. 5E). The weighted average of 17 analyses yields an age of 284 $\pm$ 7 Ma. However, the ages can be subdivided on the basis of shade of gray (in CL) of the analyzed area as follows: (1) light gray to white, showing patchy zoning, or unzoned (in some cores and all overgrowths), and (2) dark gray, showing patchy or oscillatory zoning, or unzoned (in cores). Surprisingly, the lighter areas are higher in U than the darker areas, the opposite of the usual expression of CL zoning. Grouping of age data by CL shading results in ages of 285 $\pm$ 6 and 270 $\pm$ 7 Ma. Although the uncertainties of these two ages are high, they reflect two distinct periods of growth of zircon that are correlative with episodic regional activity (discussed below). Three analyses from cores of two other zircons yield discordant older ages suggesting that these grains are xenocrysts.

Intrusive rocks

Two informally named intrusive orthogneisses, granite gneiss at Becket Hill, and granodiorite gneiss at Johnnycake Hill comprise the dated Neoproterozoic metaigneous rocks dated in the Lyme dome.

Granite Gneiss at Becket Hill.—On the Connecticut State geologic map (Rodgers, 1985), the granite gneiss at Becket Hill (Zgb) was assigned to the Potter Hill Granite Gneiss of the Neoproterozoic Sterling Plutonic Suite as defined by Hermes and Zartman (1985) from the name Sterling Plutonic Group (Rodgers, 1985). The type locality for the Potter Hill Granite Gneiss is located in the Avalon terrane in Rhode Island (Feininger, 1965), so Walsh and others (2006) use the informal name, granite gneiss at Becket Hill, because isotopically it has characteristics of the Gander terrane (Aleinikoff and others, 2007). The granite gneiss at Becket Hill intrudes the Old Lyme Gneiss. The mapped extent of the granite gneiss at Becket Hill generally corresponds to Lundgren's (1967) "sgb" biotite granite gneiss unit of his Sterling Plutonic Group.

Granite gneiss (sample OL290) was collected from an outcrop on the east side of Quarry Hill (fig. 3) from the vicinity of sample PEC-707 (Potter Hill Granite Gneiss of Zartman and others, 1988). The sampled rock is a pink to light-gray, coarse-grained, moderately foliated biotite-quartz-K-feldspar-plagioclase granite gneiss with accessory magnetite. Conventional thermal ionization mass spectrometry (TIMS) U-Pb data of

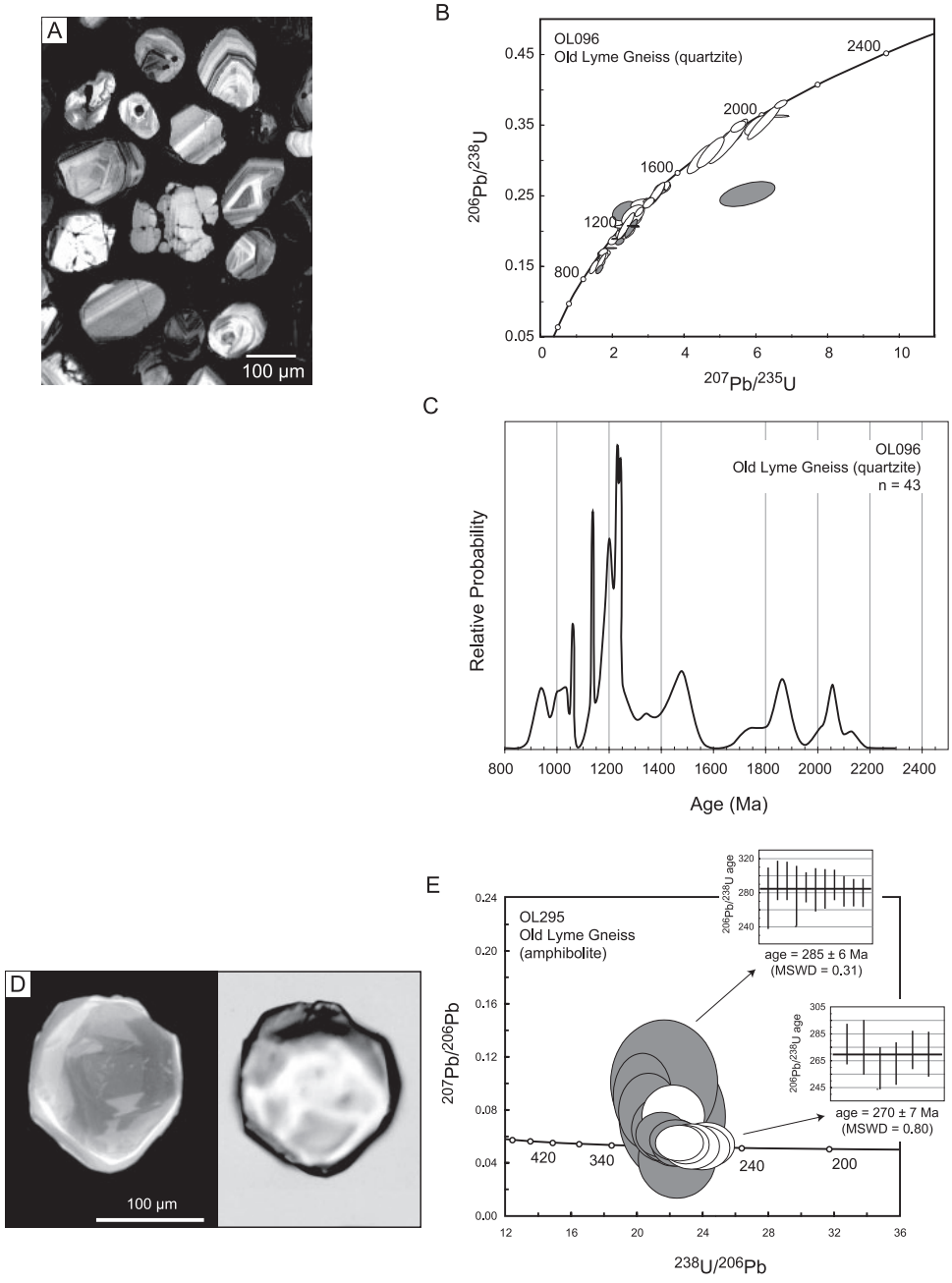

Fig. 5. Cathodoluminescent (CL) images, concordia diagrams, and probability plot from the Old Lyme Gneiss samples in this study. CL image (A) of detrital zircons and concordia diagram (B) from quartzite sample OL096. Gray ellipses in B represent discordant analyses not included in the probability plot. Relative probability plot (C) of detrital zircons from the quartzite. CL image (E) and concordia diagram (F) of metamorphic zircons from amphibolite sample OL295. Ellipses in F represent zircon appearances in CL as follows: Gray – dark gray, showing patchy or oscillatory zoning, or unzoned (in cores), white – light gray to white, showing patchy zoning, or unzoned (in some cores and all overgrowths).

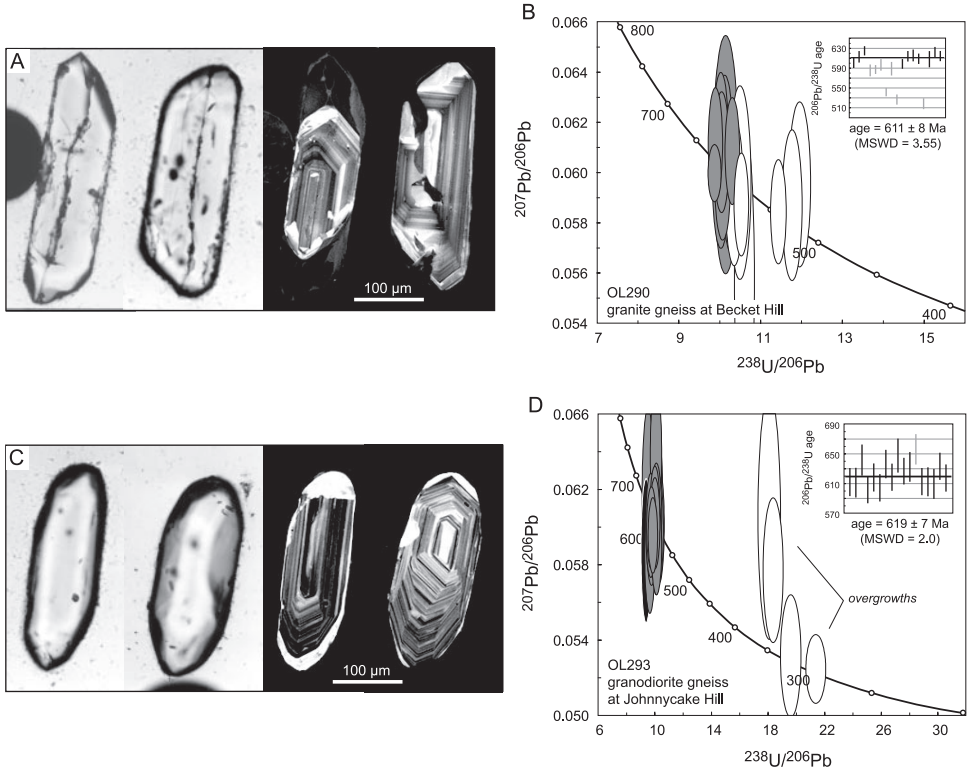

Fig. 6. Images and concordia diagrams from Neoproterozoic orthogneiss samples in this study. Transmitted light (A-left) and CL (A-right) images and concordia diagram (B) showing zircons from the granite gneiss at Becket Hill (sample OL290). Transmitted light (C-left) and CL images (C-right) and concordia diagram (D) showing zircons from the granodiorite gneiss at Johnnycake Hill (sample OL293). Gray ellipses in B and D represent cores and white ellipses represent overgrowths.

multi-grain fractions (Zartman and others, 1988) plot on or near a reference chord between 275 and 625 Ma, but are discordant and not colinear.

Zircons from sample OL290 are colorless to light brown, euhedral, and prismatic (length-to-width ratio (l/w) of 3-6). Many of the zircons are pervasively cracked, mostly parallel to the c-axes of the crystals. CL imaging shows that most grains have concentric oscillatory-zoned cores and dark, unzoned overgrowths. The character of the overgrowths varies from a thin, enveloping shell surrounding the grain (sometimes invading the core) to extensive tips (at least 50% of the grain by volume) formed on partially resorbed cores (fig. 6A). Zircon cores have moderate U contents (mostly about 200 – 500 ppm) and Th/U of about 0.5 to 1.2, typical of igneous origin. Two analyses of dark (in CL) overgrowths have high U and low Th/U, indicative of metamorphic origin (table 2).

SHRIMP isotopic data of 10 analyses form a coherent group, with a weighted average age of 611 ± 8 Ma (fig. 6B), interpreted as the time of magmatic crystallization. This age is in agreement with the interpretation of TIMS data (Zartman and others, 1988) that this rock is Neoproterozoic in age. Seven analyses of cores yielded younger Neoproterozoic ages (ca. 590 Ma, and 515 – 540 Ma; fig. 6B); two analyses of overgrowths are late Paleozoic (ca. 285 and 300 Ma). The seven analyses of Neoproterozoic age were made on oscillatory-zoned areas that are identical in appearance to zones that yielded the 611 Ma crystallization age. In addition, these analyses have U content

and Th/U that are similar to data from the older analyses. It is possible that there was either a second crystallization event at ca. 590 Ma as found in other samples regionally (Aleinikoff, unpublished data), or that the younger Neoproterozoic ages are due to Pb loss through pervasive cracks and do not represent younger events. The late Paleozoic ages of the overgrowths indicate the approximate time(s) of metamorphism.

Granodiorite gneiss at Johnnycake Hill.—The granodiorite gneiss at Johnnycake Hill is a biotite-K-feldspar-quartz-plagioclase rock exposed in the core of the Lyme dome. This orthogneiss is interpreted as a pluton because of its massive texture, because it truncates units in the Old Lyme Gneiss, and it contains xenoliths of amphibolite. This rock was not mapped by Lundgren (1967), but was briefly described (1967, p. 28) as, "quartz-dioritic and granodioritic in composition, whether volcanic or intrusive" in the lower part of his Plainfield Formation. Rodgers (1985) reinterpreted Lundgren's (1967) map and identified the rocks in the core of the Lyme dome as a mixture of Plainfield Formation (now Old Lyme Gneiss), Potter Hill Granite Gneiss, and Narragansett Pier Granite (Rodgers' unit "Zp+Zsph+Pn?"). While there are a number of dikes and irregular intrusions of migmatite and granite pegmatite similar to Narragansett Pier Granite in the core of the dome, Walsh and others (2006) mapped no rocks like the Potter Hill Granite Gneiss (now called granite gneiss at Becket Hill) in this area.

Granodiorite gneiss (sample OL293) was collected from the west side of the core of the Lyme dome (fig. 3). The rock is a moderately foliated K-feldspar-biotite-quartz-plagioclase granodiorite gneiss with trace amounts of magnetite, apatite, zircon, chlorite, and muscovite. The distribution of biotite defines a characteristic flaser texture in the gneiss. Chemically, the rock is a peraluminous calc-alkaline granodiorite (Walsh and others, 2006).

Zircons from sample OL293 are colorless to very light brown, euhedral, and prismatic (l/w = 2-4). Most grains display fine, concentric oscillatory zoning, and small overgrowths on tips (fig. 6C). Zircon cores have moderate U contents (mostly about 100 – 400 ppm) and relatively high Th/U of 0.6 to 0.9. Four analyses of overgrowths have low Th/U of 0.3 to 0.13 (table 2).

Sixteen analyses of cores yield a weighted average age of 619 ± 7 Ma (fig. 6D); one core analysis was slightly older and excluded from the age calculation. This age is interpreted as the time of crystallization of the protolith of the granodiorite gneiss. Four analyses of overgrowths yield ages of ca. 340 to 295 Ma, indicating that metamorphism occurred in the late Paleozoic.

Permian Intrusive Rocks

Permian intrusive rocks in southern New England have been known for some time. The detailed structural relationships, however, between the Permian intrusive rocks and related Alleghanian deformational events, particularly doming, have eluded earlier workers largely because of the lack of reliable modern geochronology and identification of multiple deformational fabrics, including three phases of ductile deformation in the core of the dome.

Intrusive Rocks

The three types of Permian intrusive rocks in the Lyme dome include foliated alaskite gneiss, granite pegmatite, and Westerly Granite dikes. It is necessary, however, to also review information and geochronology of a fourth unit, the Joshua Rock Granite Gneiss, which occurs east and north of the Lyme dome in the Avalon terrane (fig. 2). In this study, we re-examined the Joshua Rock Granite Gneiss at the sample locality of Zartman and others (1988) because of uncertainties regarding their zircon TIMS age.

Alaskite and Granite Gneiss.—Alaskite and granite gneiss occur as large sills and irregular intrusive bodies in the Lyme dome (fig. 3). The rock generally exhibits a well-developed foliation, but locally it is coarse-grained and poorly foliated. The

foliation developed within the gneiss has the same relative age as the dominant foliation within the host metasedimentary rocks of the Old Lyme Gneiss, and it is mapped as S1. Lundgren (1967) mapped similar rocks as units "sga", "sgba", and "sgm" of the Sterling Plutonic Group (or Suite). On the Connecticut state geologic map, Rodgers (1985) agreed with Lundgren and further subdivided Lundgren's units as Neoproterozoic Potter Hill Granite Gneiss and others as Neoproterozoic Hope Valley Alaskite Gneiss. Walsh and others (2006) suggest a compositional similarity with some of the rocks of the Neoproterozoic Sterling Plutonic Suite, but the geochronology results reported here indicate that this rock is Permian, not Neoproterozoic. Walsh and others (2006), therefore, abandoned the use of the names Sterling Plutonic Suite, Potter Hill Granite Gneiss, and Hope Valley Alaskite Gneiss for the alaskite and granite gneiss units, and instead mapped them as unnamed Permian intrusive rocks.

Alaskite gneiss (sample OL291) was collected from a belt of alaskite and granite gneiss along the west flank of the Lyme dome (fig. 3). The rock is a coarse-grained, light pink, rusty weathering quartz-plagioclase-K-feldspar gneiss with trace amounts of biotite and magnetite. At the sample site, the rock contains several thin (<10 cm) foliation-parallel screens of dark gray quartz-biotite-plagioclase gneiss that resemble the metasedimentary host rock; these screens are interpreted as deformed xenoliths. In other places in the Old Lyme quadrangle, xenoliths of paragneiss and amphibolite are present in the alaskite and granite gneiss unit and cross-cutting relationships show that the alaskite and granite gneiss cuts the host paragneiss.

Zircons from sample OL291 occur in three color varieties. Most of the zircons are dark brown, anhedral to subhedral, and equant (l/w=1). Medium brown grains (about 10% of the total zircon population) are euhedral and prismatic (l/w=3-4). Rare colorless or light brown grains are euhedral and prismatic (l/w=2-4). CL images of the medium brown grains show: (1) small, remnant cores, (2) broad, dark, patchy-zoned mantles, and (3) narrow, dark, mostly unzoned overgrowths (fig. 7A). Colorless grains show fine oscillatory zoning. Although medium brown grains are a small proportion of the total population, they were chosen for analysis because of the greater likelihood that they would yield undisturbed isotopic systematics. A few colorless grains were selected for comparison.

SHRIMP data indicate that the medium brown grains have very high U contents (about 2300 – 6000 ppm) and low Th/U of about 0.05 to 0.08 (table 2), both indicative of metamorphic origin, suggesting that this rock formed by anatexis. These grains have apparent $^{206}Pb/^{238}U$ ages of ca. 300 to 278 Ma. However, Williams and Hergt (2000) showed that high-U zircon can yield spuriously old SHRIMP $^{206}Pb/^{238}U$ ages due to instrumental bias of metamict zones. In zircons from sample OL291, it appears that zones containing greater than about 4500 ppm U yield $^{206}Pb/^{238}U$ ages that are too old (fig. 7C). Thus, to process these data, analyses were subdivided on the basis of two factors: (1) location of analysis (core or rim), and (2) U content. For analyses containing greater than about 4500 ppm U, we use $^{207}Pb/^{206}Pb$ ages (which are not affected by instrument bias). Analyses containing less than 4500 ppm U appear to have reasonable $^{206}Pb/^{238}U$ ages (fig. 7C). Colorless grains have lower U (about 600 – 1700 ppm) and higher Th/U (about 0.3 – 0.6).

Three analyses of colorless grains have Neoproterozoic ages and are interpreted as xenocrysts (fig. 7B). These data suggest that the alaskite granite gneiss was derived from Neoproterozoic basement. Analyses from all medium brown grains (cores and overgowths) plot in a limited data array with overlapping late Paleozoic ages (fig. 7B). When the data are subdivided into groups for cores and overgrowths (fig. 7C), the ages are resolved to 290 ± 4 Ma for the time of anatectic crystallization of the protolith and 279 ± 4 Ma as the time of overgrowth probably in response to subsequent high grade metamorphism.

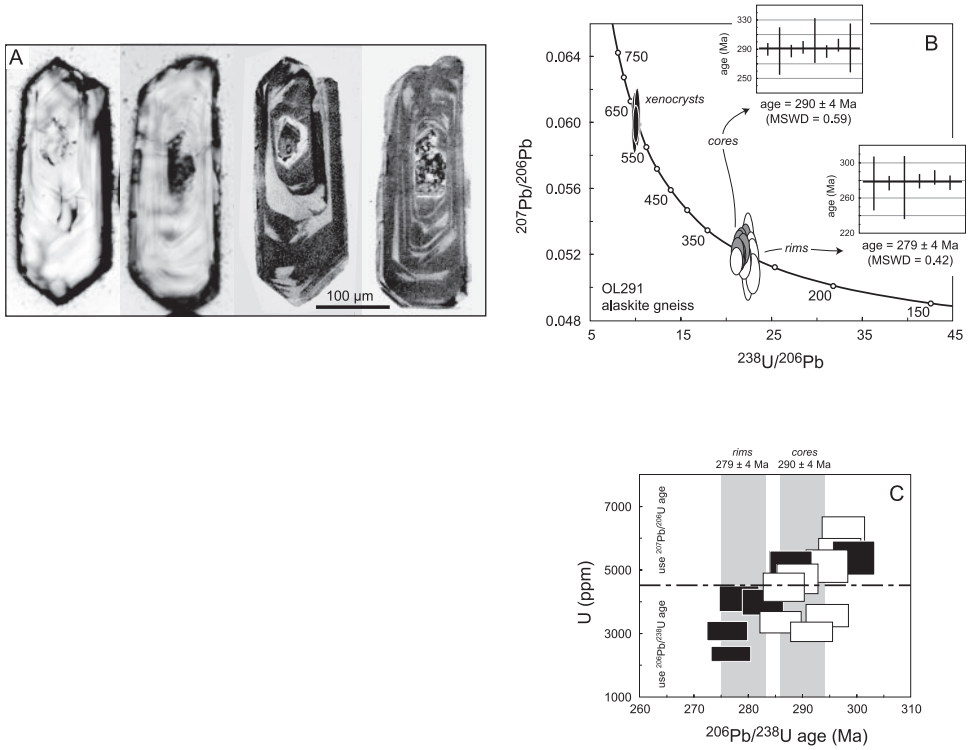

Fig. 7. Transmitted light (A-left) and CL (A-right) images and concordia diagram (B) from zircons from the alaskite gneiss (sample OL291). In B, analyses were subdivided on the basis of cores (gray ellipses), rims (white ellipses), and xenocrysts (black ellipses). (C) Plot of U content vs. age. In C, analyses containing greater than about 4500 ppm U, we use $^{207}Pb/^{206}Pb$ ages (which are not affected by instrument bias). Analyses containing less than 4500 ppm U appear to have reasonable $^{206}Pb/^{238}U$ ages.

Granite pegmatite.—Granite pegmatite occurs throughout the Lyme dome and was mapped separately where it occupied the majority of the exposed rock (Walsh and others, 2006); it occurs at virtually every outcrop. Lundgren (1967, p. 21) mapped 15 pegmatite bodies on the east flank of the Lyme dome as informally named "Black Hall type" granite pegmatite. He reported that the pegmatite, although largely unmapped, occupied 25 percent of the core of the Lyme dome, and we generally agree with this estimate. Rodgers (1985) assigned the pegmatite in the core of the Lyme dome to the Narragansett Pier Granite ("Pn" on the State map) after usage in Rhode Island (Nichols, 1956; Feininger, 1968). Walsh and others (2006) mapped the rocks as unnamed granite pegmatite because they are not contiguous with mapped Narragansett Pier Granite in southeastern Connecticut and Rhode Island.

The granite pegmatite occurs as late straight-walled tabular dikes and older non-foliated to weakly foliated irregular intrusive migmatite bodies in the Lyme dome (fig. 8). In general, the irregular intrusive bodies are sills that intruded sub-parallel to the dominant foliation (S1) in the country rocks or irregular masses that post-date the development of S1. The younger, tabular dikes are generally steeply dipping, but some shallowly dipping dikes were also observed (fig. 8; Walsh and others, 2006). The dikes in the Old Lyme quadrangle have a preferred east-west orientation (fig. 8, Walsh and others, 2006). Hozik (1988) notes a similar E-W trend for most of the Narragansett Pier Granite dikes and the largest Westerly Granite dikes in Rhode Island.

Pegmatite (sample OL294B) was collected from a medium- to coarse-grained, weakly foliated, light-pink to pink and white discordant sill at Point O'Woods on Long

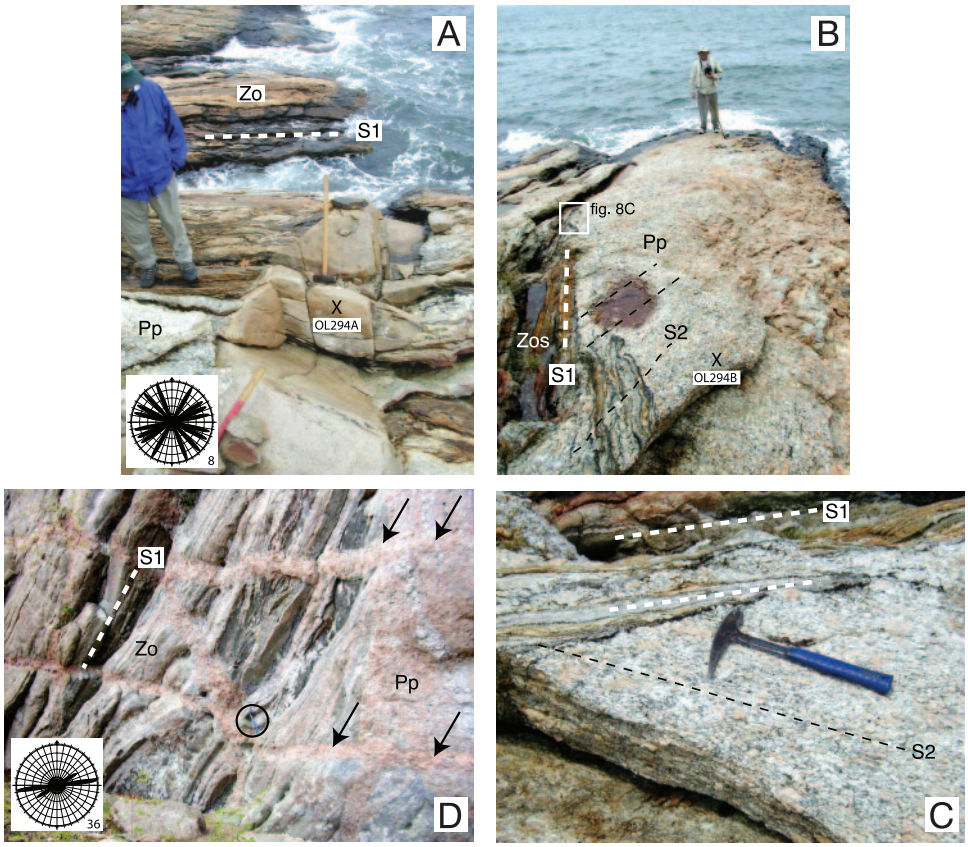

Fig. 8. Photographs of Permian intrusive rocks in the Old Lyme quadrangle. (A) Westerly Granite dike in the Old Lyme Gneiss at Point O'Woods (sample site for OL294A shown by X). Inset figure is a rose diagram showing the strike of 8 dikes. (B) Medium- to coarse-grained Permian granite pegmatite in the Old Lyme Gneiss at Point O'Woods (sample site for OL294B shown by X). The pegmatite is finer grained to the east (left). The black dashed line shows the trace of weakly developed S2 cleavage in the pegmatite and Old Lyme Gneiss. White inset rectangle shows the location of photograph in fig. 4C. (C) Close-up view of the S2 foliation in the pegmatite and the truncation of S1 in the Old Lyme Gneiss. (D) Dikes of Permian granite pegmatite in the Old Lyme Gneiss; circle shows hammer. The gently dipping dikes post-date the steeply dipping dikes in this photo (see arrows). Inset figure is a rose diagram showing the principal east-west strike of 36 steeply dipping dikes seen in the area. Rock unit abbreviations: Neoproterozoic Old Lyme Gneiss sillimanite schist (Zos) and biotite gneiss (Zo), and Permian granite pegmatite (Pp). The trace of the dominant foliation in all photos is S1 and is shown by a white dashed line. Rose diagrams and stereonets in this and subsequent figures compiled with Structural Data Integrated System Analyzer software (DAISY) by Salvini (2004).

Island Sound (figs. 3 and 8). The rock is a K-feldspar-plagioclase-quartz-biotite pegmatite with trace amounts of chlorite replacing biotite, and muscovite replacing K-feldspar. The sample is weakly deformed and contains the regional S2 dome-stage foliation as a weakly developed cleavage (fig. 8). The pegmatite clearly post-dates the regional S1 foliation in the host rocks (fig. 8). Chemical analysis of sample OL294B shows that it is peraluminous calc-alkaline granite (Walsh and others, 2006).

Zircons from sample OL294B are medium to dark brown, euhedral, and prismatic (l/w=3-6, and some acicular grains with l/w=8-10). In CL, the grains show concentric oscillatory zoning, with small, unzoned overgrowths (fig. 9A). Some grains contain partially resorbed cores. Zoned regions have variable U (about 375 – 1670 ppm) and low Th/U (0.07 – 0.18) (table 2). Monazite is yellow to orange, anhedral to subhedral,

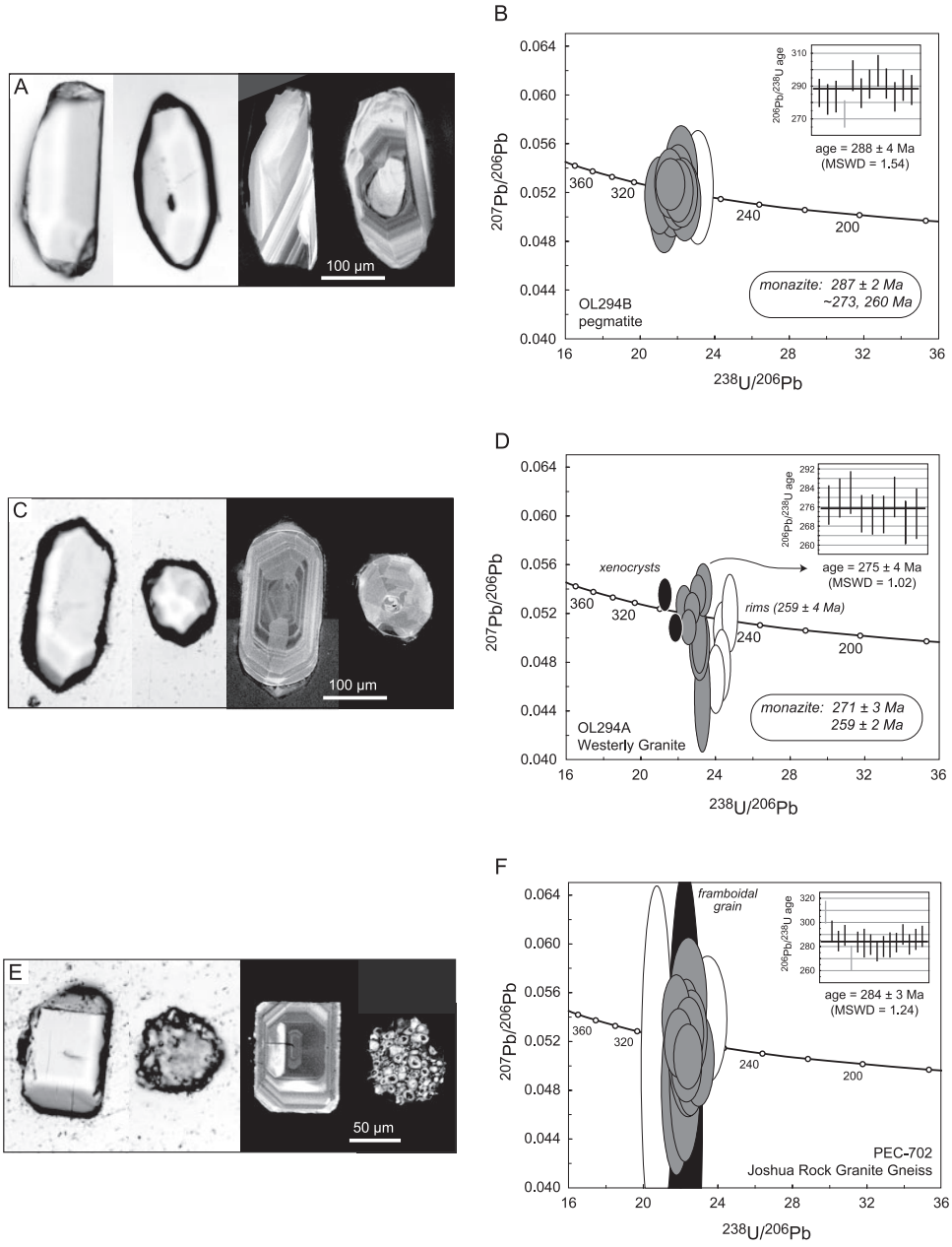

Fig. 9. Images and concordia diagrams from Permian granitic rocks in this study. Transmitted light (A-left) and CL (A-right) images and concordia diagram (B) showing zircons from the granite pegmatite (sample OL294B). Transmitted light (C-left) and CL images (C-right) and concordia diagram (D) showing zircons from the Westerly Granite dike (sample OL294A). Monazite ages are summarized in the lower right of B and D. Transmitted light (E-left) and CL (E-right) images and concordia diagram (F) showing zircons from the Joshua Rock Granite Gneiss (sample PEC-702). In B and D, gray ellipses represent cores, white ellipses represent overgrowths, and black ellipses represent xenocrysts (D). In F, gray ellipses are cores used in the age calculation, white ellipses are cores excluded from the age calculation, and the black ellipse is a framboidal zircon.

and equant (l/w=1). In backscattered electrons imaging (BSE), monazite shows a variety of zoning patterns, including euhedral oscillatory, spotty, and patchwork; some grains are unzoned.

Eleven analyses of zircon yield a coherent group with a weighted average age of 288 ± 4 Ma (fig. 9B). One analysis is slightly younger at ca. 273 Ma. Seven analyses of monazite cores yield an age of 287 ± 2 Ma. Ten additional analyses of monazite yield younger ages, suggesting subsequent monazite growth also at ca. 273 and 260 Ma.

Westerly Granite dikes.—The Westerly Granite occurs as straight-walled, undeformed tabular dikes that intrude all units in the Lyme dome (fig. 8). We correlate these dikes with the Westerly Granite of Gregory (1906) and Feininger (1963). Westerly Granite dikes were observed at eight locations in the Old Lyme quadrangle (Walsh and others, 2006). The dikes are generally steeply dipping (47° – 82°) with variable strikes (fig. 8). The dikes range in thickness from 0.1 to 2 meters. Lundgren (1967) noted that the dikes exposed at Point O'Woods have a generally east-northeast trend. Goldsmith (1988) and Zartman and Hermes (1987) noted that Westerly Granite dikes in southeastern Connecticut and southern Rhode Island also have variable strikes, but locally have generally east-west trends with dips that are moderate to gentle to the south-southeast — gentler than observed in the Old Lyme area. Goldsmith (1988) also noted that large dikes observed in quarries generally have irregular contacts, and are not straight-walled tabular features like those seen in smaller outcrops. Mapping by Goldsmith (1967a, 1967b, 1967c, 1985b) identified many map-scale Westerly Granite dikes, up to several kilometers long and tens of meters thick, in southeastern Connecticut. In the immediate area of Old Lyme, the map-scale dikes are limited to the coastal area along Long Island Sound (Rodgers, 1985; Zartman and Hermes, 1987; Goldsmith, 1988) (fig. 2). East of the Old Lyme quadrangle, larger intrusions occur farther north and into Rhode Island where Hermes and others (1994) assigned them to the fine-grained granite of the Narragansett Pier Plutonic Suite.

Field evidence shows that the Westerly Granite dikes post-date most of the granite pegmatite and all ductile structures in the deformed rocks (fig. 8). Locally, the margins of the Westerly Granite dikes are characterized by large megacrysts of K-feldspar up to 15 cm long. These dikes have gradational margins with the granite pegmatites, and their similar chemistry, similar age, and the local gradational margins between the two suggest that the Westerly is closely related to some of the granite pegmatite. Earlier workers linked the Westerly Granite with the Narragansett Pier Granite based on similar ages and chemistry (Lundgren, 1967; Buma and others, 1971; Zartman and Hermes, 1987; Goldsmith, 1988; Skehan and Rast, 1990; Hermes and others, 1994).

Granite (sample OL294A) was collected from a 0.8-m-thick dike at Point O'Woods on Long Island Sound (figs. 3 and 8). The dike is a light-pink, fine-grained, equigranular K-feldspar-plagioclase-quartz-biotite granite with accessory muscovite after K-feldspar, chlorite replacing biotite, and opaque minerals including magnetite. Contacts with the host rock (granite pegmatite and Old Lyme Gneiss) are straight-walled and sharp (fig. 8). The dike strikes 276° and dips at 59°. Chemical analysis of the dike shows that it is a peraluminous calc-alkaline granite (Walsh and others, 2006).

Sample OL294A yielded a small amount of zircon and abundant monazite. Zircons are quite variable in appearance; they are colorless to medium brown, euhedral, and stubby to elongate (l/w=1-6). In CL, the grains show concentric oscillatory zoning (fig. 9C). Many grains have significant dark (in CL) overgrowths. The heterogeneous zircon population suggests that this Westerly Granite dike contains xenocrystic zircons, assimilated during derivation and/or intrusion. Monazite is pale yellow to light orange, anhedral to subhedral, and equant (l/w=1). Zircon cores and tips interpreted as igneous in origin have variable U content (about 100 – 1200 ppm) and Th/U (0.19 – 1.13) (table 2).

Zircons with a variety of morphologies were prepared for SHRIMP analysis because of the very low yield from our Westerly Granite dike sample. Interpretation of the results is difficult because the data do not conform to the normal relationships of zoning, spot location, age, and Th/U. For example, some dark overgrowths, of presumed metamorphic origin, have uncharacteristically high Th/U and the same age as oscillatory-zoned cores. Some oscillatory-zoned cores have uncharacteristically very low Th/U. Thus, lacking objective textural criteria to define groups, we somewhat subjectively subdivide the data set based entirely on ages. Nine analyses form an apparent coherent group with a weighted average age of 275 ± 4 Ma (fig. 9D). Two analyses yielded slightly older ages of ca. 288 and 295 Ma. Four younger rim-ages are grouped with an age of 259 ± 4 Ma. One rounded core has a $^{207}Pb/^{206}Pb$ age of 1401 Ma (table 2). Monazite ages provide support for our zircon data, although these data also are grouped primarily by age. Analyses of three cores and one rim yield an age of 271 ± 3 Ma, whereas ten analyses (4 cores, 6 rims) result in an age of 259 ± 2 Ma. We suggest that the Westerly Granite dike was emplaced at ca. 275 Ma and reheated at ca. 259 Ma. TIMS data from multi-grain fractions of zircon from Westerly Granite in Graniteville, Connecticut (about 10 km northeast of sample OL294A) indicate a lower intercept (crystallization) age of 276 ± 7 Ma, plus inheritance from Proterozoic or Archean sources (Zartman and Hermes, 1987). See discussion about the significance of the old ages in the Extension section of the Tectonic Model below.

Joshua Rock Granite Gneiss.—The Joshua Rock Granite Gneiss is an aegerine-augite granite that occurs entirely within the Avalon terrane (fig. 2). Since we believe it is involved in the same structures that occur within the Lyme dome, we have chosen to include a discussion of the age and intrusive history here. The type locality is at a quarry at Joshua Rock (fig. 2) on the Connecticut River in the Deep River quadrangle (Lundgren, 1963), but we have chosen to re-analyze a sample from the location which Zartman took his sample (Zartman and others, 1988).

The Joshua Rock Granite Gneiss was originally mapped as an interlayered member of the New London Gneiss (Lundgren, 1963, 1966b; Goldsmith, 1967a, 1967b, 1967c). The State map (Rodgers, 1985) shows five map units of Joshua Rock Granite Gneiss as an interlayered member of the Waterford Group, with occurrences north and east of the Lyme dome in the Avalon terrane (fig. 2). Synder (1964) described a similar rock at a small, single locality within alaskite gneiss in the northern part of Montville, east of Gardner Lake, in the Fitchville quadrangle, but this locality was not included as Joshua Rock on the State map by Rodgers (1985). The Joshua Rock Granite Gneiss was considered Neoproterozoic by Rodgers, but Ordovician or younger by Goldsmith (1967b, 1967c). When he mapped it, Goldsmith suggested that the Joshua Rock may be younger than the Neoproterozoic New London Gneiss. Zartman and others (1988) suggest that Rodgers (1985) mapped it as a member of the New London Gneiss because the two units apparently contained the same structural fabrics.

The granite (sample PEC-702) is from the collection of Zartman and others (1988) (fig. 2). The mildly peralkaline granite, is medium-grained, and composed of K-feldspar-plagioclase-quartz with accessory pyroxene, allanite, opaque minerals, sphene, and fluorite (Zartman and others, 1988). The sample was collected from a roadcut at the Crystal Mall shopping center on Route 85 (Zartman and others, 1988) in the southern part of the Montville quadrangle (Goldsmith, 1967c). Zircons were re-analyzed by SHRIMP in this study because of uncertainties regarding the TIMS zircon age by Zartman and others (1988). The Joshua Rock Granite Gneiss at the sample location intrudes the New London Gneiss, and contains a planar foliation that is "parallel to the structural trend of the Alleghanian orogeny" (Zartman and others, 1988, p. 392). Goldsmith (1961) interpreted this belt of rock as a phacolith. At the sampled roadcut, the granite contains a very weak, wispy foliation that is generally parallel to the dominant fabric in the amphibolite country rock (local S1). The

dominant fabric appears to be partially to totally annealed or resorbed in places, leaving remnant schlieren of biotite and hornblende as selvages. The amphibolite at the contact with the granite gneiss contains abundant granitic leucosomes and thin, foliation-parallel to slightly discordant intrusive sills suggesting that host rock was injected during, or very late in the development of S1. Zartman and others (p. 398, 1988) stated that, "it is ambiguous whether the rock exhibits well preserved igneous texture or if the rock has been completely annealed and is nearly strain free due to high temperature recrystallization." Second generation folds (local F2) and weak foliation (local S2) deform the Joshua Rock Granite Gneiss, and several S-shaped and Z-shaped folds are present at the roadcut and are outcrop-scale examples of the large "S" fold on the Connecticut State geologic map (Rodgers, 1985) (fig. 2). The local orientations of the F2 folds and S2 foliation generally strike east-west, dip steeply, and differ from the orientations seen in the Old Lyme quadrangle where they dip steeply but strike northeast (see section on D2 below).

Most of the zircons from sample PEC-702 are anhedral and appear to be amalgamations of many small grains. In CL, these grains have a framboidal texture (fig. 9E). Less than one percent of the zircon population is composed of blocky (l/w=1), colorless, euhedral grains that have concentric oscillatory zoning in CL. The co-existence of these very different zircon morphologies is related to magma composition. Zircons from peralkaline rocks commonly are anhedral (Aleinikoff and Stoeser, 1989, and references therein) because they form late in the melt crystallization sequence due to the high solubility of zircon in peralkaline magma (Watson, 1979; Watson and Harrison, 1983). In metaluminous rocks, zircons crystallize early, due to low zircon saturation of the melt, and therefore usually are euhedral. It is possible that the few euhedral zircons from this sample formed in limited pockets of melt that had locally evolved to metaluminous composition, whereas the majority of zircon (of framboidal morphology) formed late in the peralkaline melt crystallization history. Despite being only a tiny percentage of the total zircon population, the colorless, euhedral grains were chosen for SHRIMP analysis because they are less complicated and more typical of igneous zircons than the framboidal zircons.

Fourteen analyses (from 13 euhedral grains and one framboidal grain, for comparison) form a coherent group with an age of 284 ± 3 Ma (fig. 9F). One analysis is somewhat older (ca. 310 Ma) and one analysis is slightly younger (ca. 270 Ma). Zartman and others (1988) analyzed one multi-grain fraction composed entirely of colorless euhedral grains and obtained slightly discordant data with a $^{207}Pb/^{206}Pb$ age of 280 Ma. Three other fractions yielded slightly older ages (326 – 297 Ma; Zartman and others, 1988). We conclude that the Joshua Rock Granite Gneiss crystallized at 284 ± 3 Ma.

Structural Geology of Ductile Fabrics

Three generations of planar and linear ductile fabrics, from oldest to youngest, D1 to D3, are recorded in rocks of the Lyme dome. A fourth deformation event, D4, is recognized by late, randomly oriented tabular cross-cutting dikes of pegmatite. No ductile fabrics are associated with D4.

D1

The oldest ductile deformational event (D1) is characterized by a penetrative gneissosity (S1) that is the dominant planar foliation in most rocks, and is the dominant foliation that is deformed by the Lyme dome (fig. 10). Locally S1 is axial planar to rootless, outcrop-scale isoclinal folds (F1) that deform a now relict gneissic compositional layering (S0) that is parallel to bedding in the metasedimentary rocks and some amphibolites (fig. 11). The relict gneissic layering (S0) is absent in the intrusive rocks. The S1 gneissosity pre-dates emplacement of the Westerly Granite and Permian granite pegmatite but post-dates the Silurian metasedimentary rocks in the

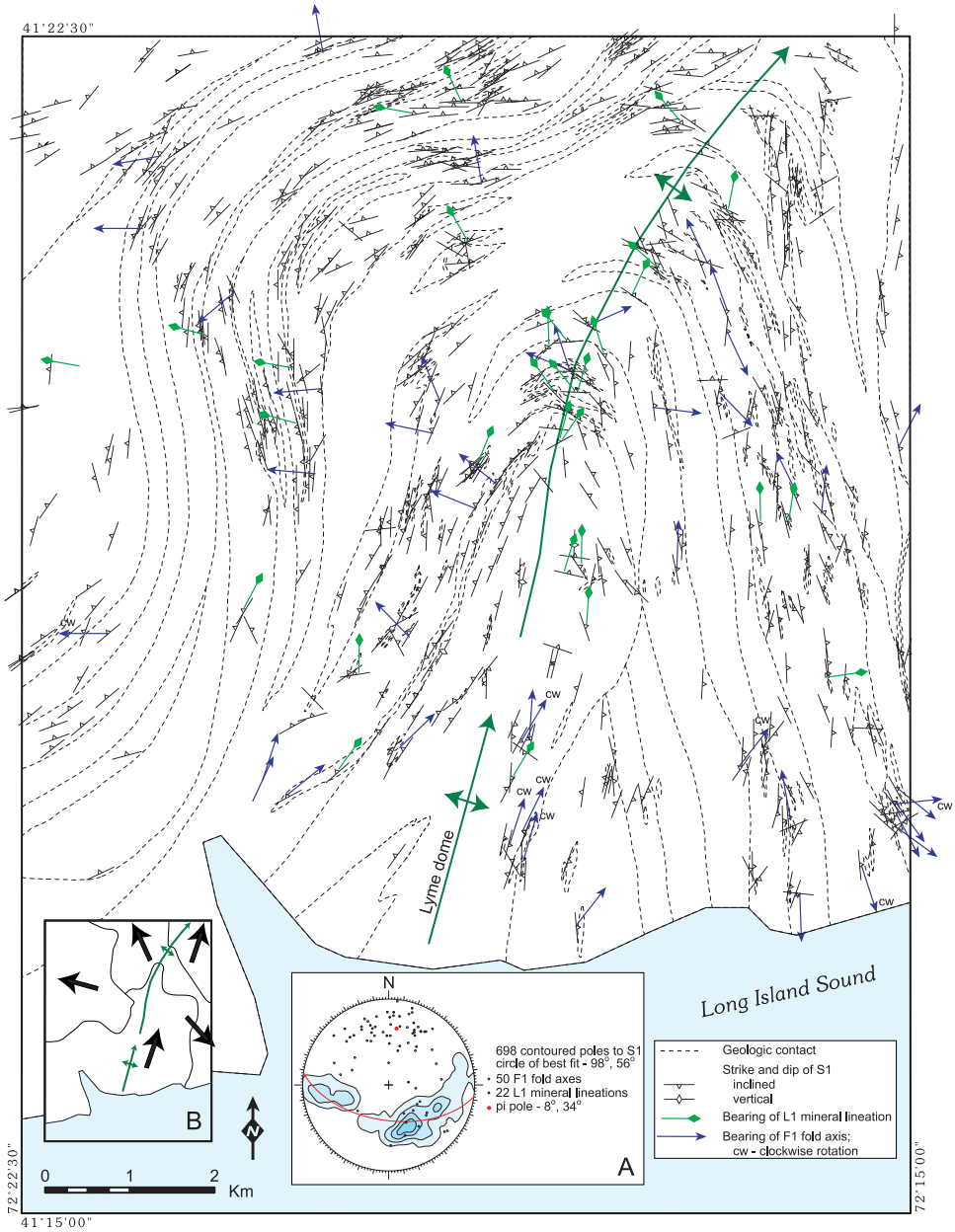

Fig. 10. Map of D1 structures in the Old Lyme quadrangle showing S1 foliation, L1 mineral lineations, F1 fold axes, and axial trace of the Lyme dome. Inset diagram (A) shows a lower hemisphere equal area projection of contoured poles to S1, L1 and F1 linear elements, pi pole to folded S1, and the great circle of best fit to folded S1. Contour interval is 2 percent. Inset map (B) shows a summary diagram with the generally radial trends of F1 and L1 in domains across the Lyme dome.

Hunts Brook slice (Wintsch and others, 2007) between the Lyme dome and the Selden Neck block. The S1 gneissosity is folded by the Lyme dome, and poles to S1 define a great circle whose π pole plunges moderately to the north (fig. 10). F1 fold axes generally plunge down the dip of the foliation. The bearing and plunge of F1 fold axes

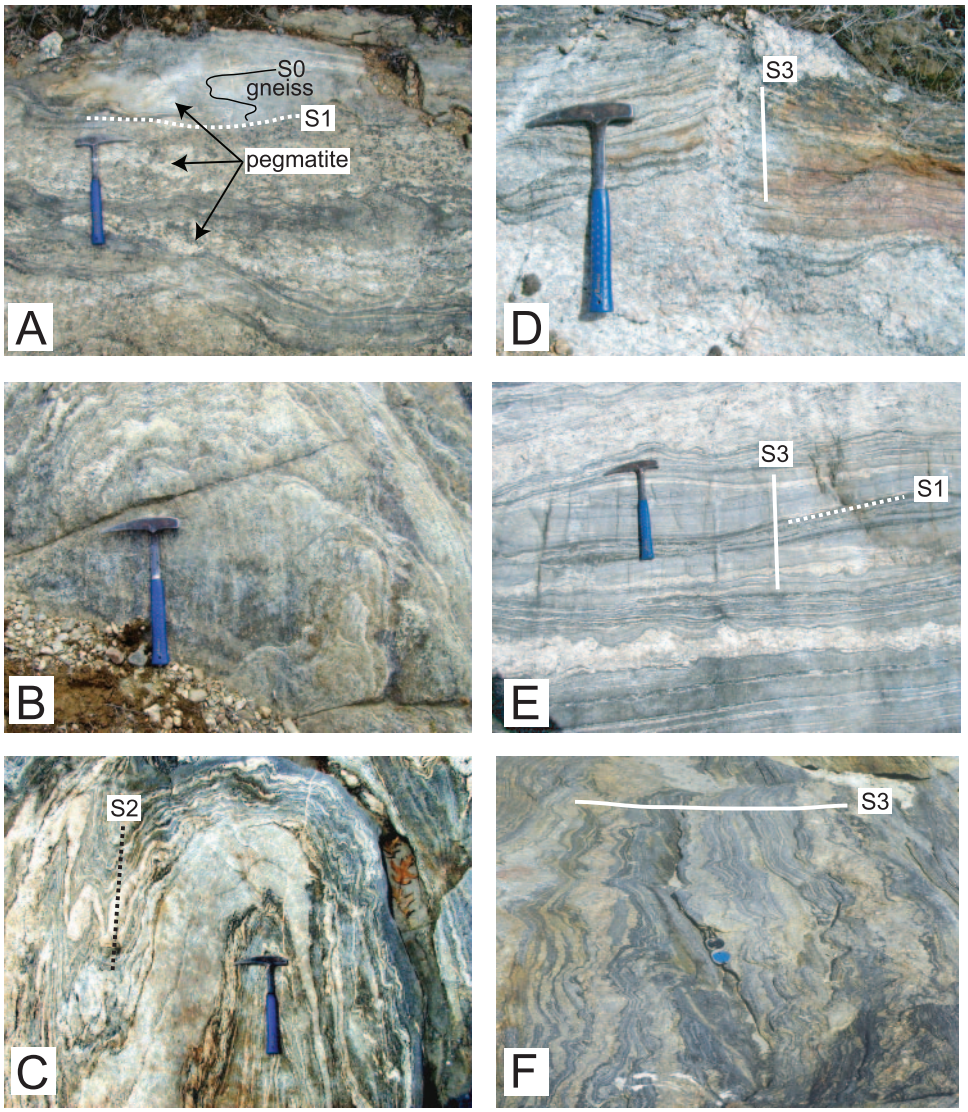

Fig. 11. Photographs of deformational fabrics in the Lyme dome. (A) F1 fold of S0 compositional layering showing axial planar S1 foliation. Pegmatite leucosomes form parallel to both S1 and S0. (B) Down-dip L1 mineral lineations in Old Lyme Gneiss. (C) Upright F2 folds with S2 foliation deform S1 gneissosity in the Old Lyme Gneiss. Migmatitic leucosomes and granitic gneiss are parallel to S1. (D) Permian granite pegmatite intruded parallel to S3. (E and F) Boudinage, or pinch and swell structure parallel to S3 in Old Lyme Gneiss deforms S1 (photo F by J. R. Stone).

varies across the map, and shows a somewhat radial pattern around the Lyme dome (fig. 10). Most observed F1 folds are isoclinal with an indeterminate asymmetry, but some F1 folds with clockwise rotations are seen on the east flank of the dome (fig. 10). Elongation and mineral cluster lineations in the plane of S1 (L1) consist of quartz, plagioclase, K-feldspar, hornblende, and rare sillimanite, and, like the F1 fold axes, generally trend steeply down the dip of S1 and show a radial trend around the dome (figs. 10 and 11). Rare L1 sillimanite occurs as quartz-sillimanite, or quartz-fibrolite, grain cluster lineations.

D2

The second deformational event (D2) is characterized by a variably developed cleavage and schistosity. This foliation, called S2, is well developed in the schistose rocks and poorly developed to not present in the more competent quartzo-feldspathic gneissic or pegmatitic rocks. Where S2 is present in the gneissic or post-S1 pegmatitic rocks, it is a spaced cleavage (fig. 8). The S2 foliation pre-dates intrusion of the Westerly Granite and most exposures of the granite pegmatite. Where the granite pegmatite is finer grained, it is locally deformed and contains the S2 foliation as a weakly developed cleavage (fig. 8). Locally S2 is axial planar to outcrop-scale, upright, tight to open folds (F2) that deform the dominant gneissic fabric (S1) and older F1 folds. The F2 folds are not apparent in post-S1 intrusive rocks because there is no older planar fabric (S1) to show the folding. These folds are axial planar to the Lyme dome (figs. 11 and 12). The average strike and dip of the S2 foliation is 8°, 85° (fig. 12). The average bearing and plunge of F2 fold axes and S1/S2 intersection lineations is 16°, 26°, and matches the orientation of the π pole (8°, 34°) to the great circle of deformed S1 gneissoisty (figs. 10 and 12). The F2 fold axes generally plunge to the north, but southward plunges occur locally, especially in the southeastern part of the Old Lyme quadrangle along the coast. Locally asymmetric F2 folds are seen with both clockwise and counter-clockwise rotation senses (fig. 12). Most clockwise folds occur on the west flank of the dome, and most counter-clockwise folds occur on the east flank of the dome, consistent with a model of parasitic folds developed by flexural flow (flanks of the dome moved up relative to the core) in a buckle anticline (Dixon, 1987; Burg and others, 2004). Elongation and mineral lineations in the plane of S2 (L2) consist of quartz, sillimanite, biotite, and/or K-feldspar and are generally parallel to the F2 fold axes, and also generally plunge to the north (fig. 12). Sillimanite L2 lineations commonly occur as aggregates of needles.

D3

The third deformational event (D3) is characterized by boudinage and weak folding with associated spaced cleavage development (fig. 11). The foliation, called S3, is well developed in the layered schistose and gneissic rocks and poorly developed to not present in the more massive gneissic rocks and young granites and pegmatites. Layered gneiss and amphibolite typically display parting along S3 (fig. 11). The S3 foliation was not observed in the Westerly Granite and the Permian granite pegmatite because the cleavage is not penetrative. Pegmatite dikes, however, locally intrude parallel to the S3 cleavage in boudin necks suggesting that some of the dikes utilized the cleavage during intrusion (fig. 11). Locally S3 is axial planar to upright, broad to open folds (F3) that are associated with boudinage or pinch-and swell structure (fig. 11). The S3 cleavage and F3 folds generally deform the dominant gneissic fabric (S1), but terminate within the granitic and pegmatitic layers within the metasedimentary rocks. The average strike and dip of the S3 cleavage is 259°, 87° (fig. 13), or slightly south of due west and is virtually the same trend observed for the strike of the steeply dipping granite pegmatite dikes (fig. 8D). The average bearing and plunge of F3 fold axes and intersection lineations is 51°, 40°, but these linear elements show some variability due to the pre-existing orientation of S1 (fig. 13).

DISCUSSION

In this section we integrate mapping, structural analysis, and geochronology with the metamorphic history of the rocks by modeling the pressure-temperature time path. We also present a tectonic model that explains the Neoproterozoic deposition and intrusion of the rocks in the core of the Lyme dome, and the major late Paloeozoic events of Alleghanian orogenesis. Finally, we present the mechanisms of dome formation and their relationship to the crustal evolution of southern Connecticut.

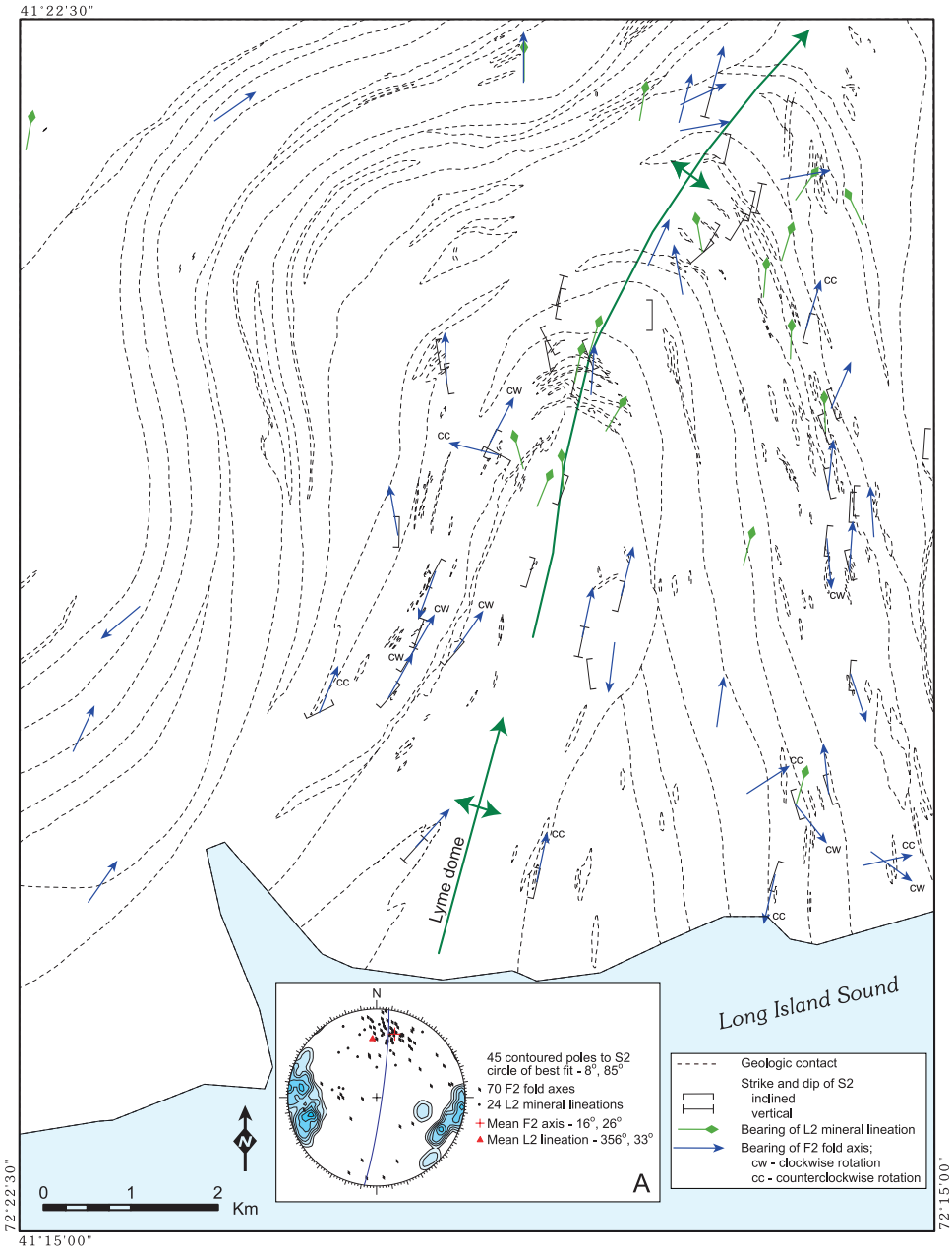

Fig. 12. Map of D2 structures in the Old Lyme quadrangle showing S2 foliation, L2 mineral lineations, F2 fold axes, and axial trace of the Lyme dome. Inset diagram (A) shows a lower hemisphere equal area projection of contoured poles to S2, L2 and F2 linear elements, S2 plane of best fit, and mean F2 axis and L2 lineation. Contour interval is 2 percent.

Pressure-Temperature-Time-Deformation Path

The new U-Pb crystallization ages of zircon and monazite reported above, provide the absolute times of deformation in this area. These can be reconciled with the overall metamorphic history of these rocks by applying the P-T-t (pressure-temperature-time)

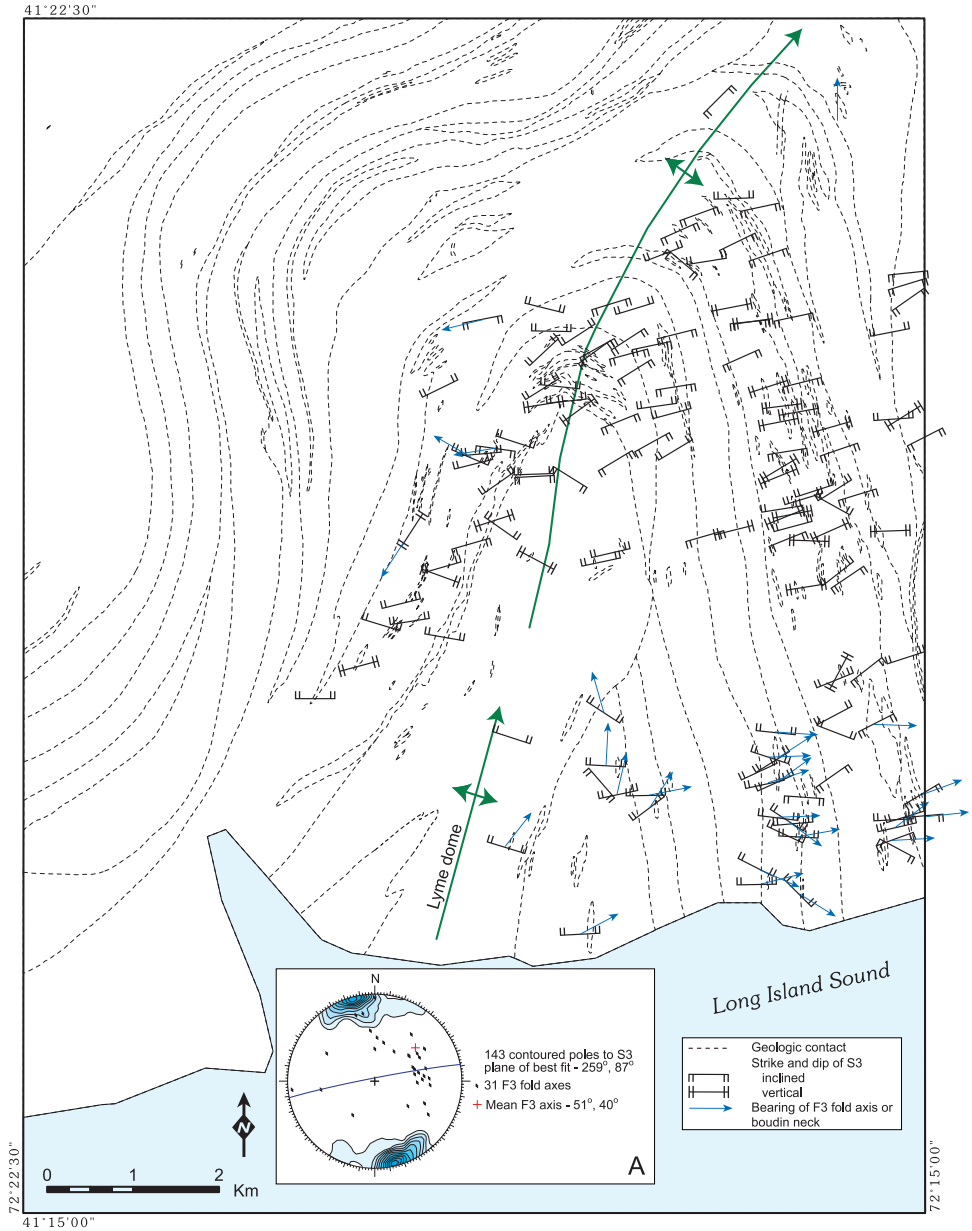

Fig. 13. Map of D3 structures in the Old Lyme quadrangle showing S3 foliation, F3 fold axes, and axial trace of the Lyme dome. Inset diagram (A) shows a lower hemisphere equal area projection of contoured poles to S3, F3 fold axes, S3 plane of best fit, and mean F3 axis. Contour interval is 2 percent.

paths calculated by Wintsch and others (2003). These one-dimensional thermal calculations were constrained by the cooling rates in rocks of the Bronson Hill terrane in the Essex quadrangle to the west. Values for heat capacity, thermal conductivity, radioactive heat generation and mantle heat flux were taken from the literature. Uniform rates of loading and unloading from four positions in a north-south traverse along this terrane from northern to southern Connecticut were found to satisfy the

geochronologic data all along the traverse. Times and rates of cooling were constrained by $^{40}Ar/^{39}Ar$ thermochronology, U-Pb geochronology, and by metamorphic P-T conditions from the literature. Multiple iterations with trial times and rates of loading and unloading and residence times identified particle paths that satisfied the data. The modeled metamorphic history identifies the particle (crustal) path of the present erosion surface, and predicts the paths for rocks structurally above (and now eroded from) the present erosion surface, and of those still below the present erosion surface.

The results of the modeled P-T-t path of Wintsch and others (2003) are summarized with temperature-time lines and loading and exhumation time lines (figs. 14 and 15), and with the derived pressure-temperature-time lines (PTt) calibrated here for absolute time (fig. 15). The model PTt paths cross the following critical reaction boundaries shown in figures 14 and 15 (compiled from Holdaway and Mukhopadhyay, 1993; Spear and others, 1999; and Vielzeuf and Schmidt, 2001):

$$\text{Ab} + \text{Kfs} + \text{Qtz} + \text{V} = \text{liquid} \quad (1)$$

$$\text{Ms} + \text{Pl} + \text{Qtz} = \text{Kfs} + \text{As} + \text{liquid} \quad (2)$$

$$\text{Bt} + \text{As} + \text{Pl} + \text{Qtz} = \text{Grt} + \text{Kfs} + \text{liquid} \quad (3)$$

$$\text{Bt} + \text{Pl} + \text{Qtz} = \text{Opx} + \text{Kfs} + \text{liquid} \quad (4)$$

$$\text{Bt} + \text{As}(+ \text{Pl} + \text{Qtz}) = \text{Grt} + \text{Crd} + \text{liquid} \quad (5)$$

$$\text{Kyanite} = \text{Sillimanite} \quad (6)$$

The modeling results most relevant to this study lie between the 15 km (dotted line) and 20 km (dashed line) isopleths (fig. 14). The model ignores the heat advected by the Westerly and Joshua Rock granitic rocks that intruded directly into the rocks studied. Their volume and thermal mass is small, however, and their temperatures would have been close to the ambient anatectic temperatures of their host rocks, and so their effect on the model would be minimal, especially in view of the divariance of the reactions (for example, Spear and others, 1999).

The earliest stage of deformation (D1) identified in this study produced a penetrative foliation (S1) and layer-parallel migmatite. This occurred at ca. 290 Ma, at metamorphic conditions consistent with the beginning of melting, and generally consistent with the mineralogy of the D1 structures (fig. 14A). These conditions are predicted to have occurred in the kyanite zone, and Lundgren (1967, p. 14) reported relict kyanite as a "rare accessory mineral" in two samples of his pelitic "biotite-sillimanite schist and gneiss" map unit. In fact, modeling shows that much of the early partial melting occurred in the kyanite zone (fig. 15).

The second deformation (D2) was folding associated with the dome, and development of overprinting S2 fabrics. These fabrics are only moderately well preserved in granitic pegmatites, one of which is dated at ca. 288 Ma (see Results section on granite pegmatite above). The same folding event deforms the Joshua Rock Granite Gneiss (fig. 2) dated at ca. 284 Ma, showing that this deformation outlasted the intrusion. Moreover, the magmas must have intruded from deeper sources, so that the P-T conditions of the melting were higher than those near the 15 km isopleths of figures 14 and 15. The elongate ellipses with the black arrows (figs. 14 and 15) show the possible source conditions of these magmas. To the extent that some of these magmas did intrude from below, this event probably advected heat to these rocks. Crystallization of metamorphic zircons in the amphibolite (see Results section on Old Lyme Gneiss, sample OL295) may have occurred during this event. Petrography indicates that idioblastic to poikiloblastic garnet grew during or subsequent to the D2 event, and

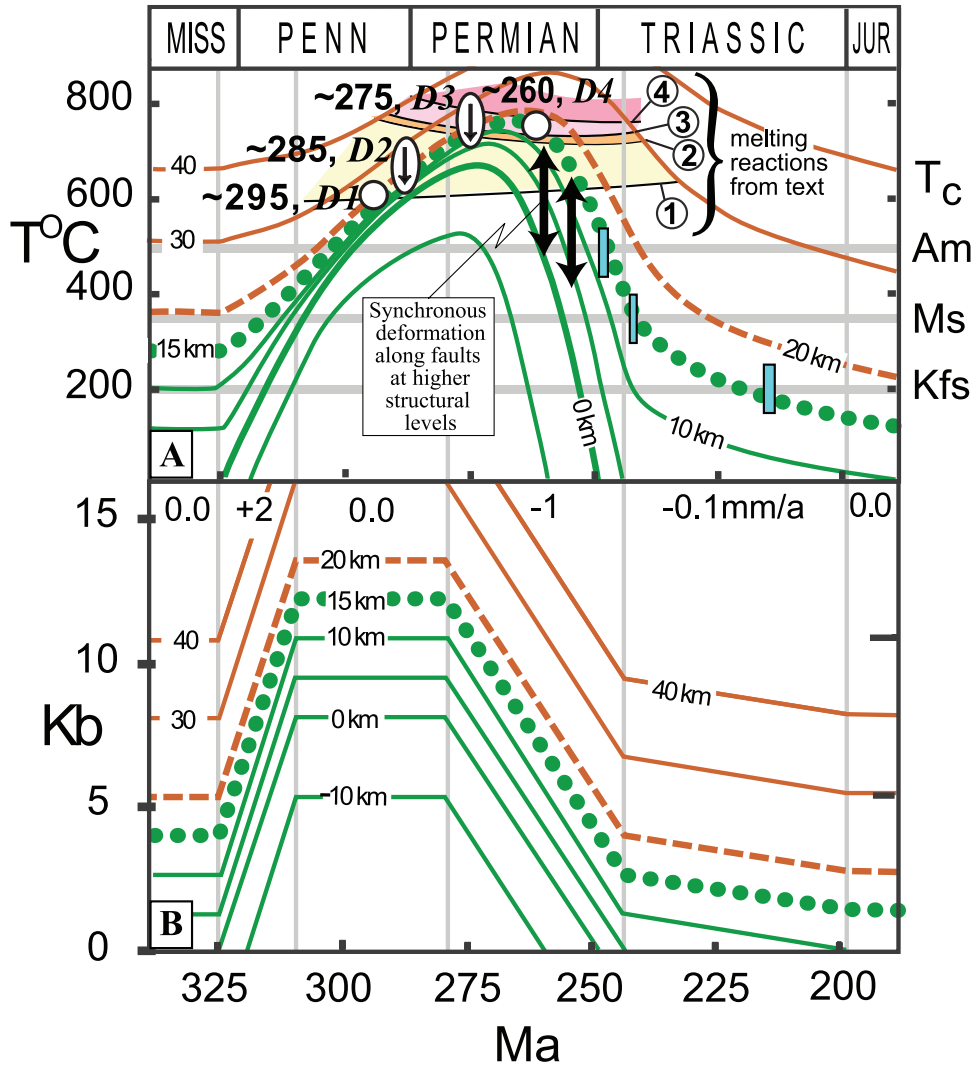

Fig. 14. Model thermal history (A) and loading and exhumation history (B) for coastal Connecticut, constrained by regional geochronology and local thermochronology (Wintsch and others, 2003). Amphibole (Am), muscovite (Ms), and K-feldspar (Kfs) $^{40}Ar/^{39}Ar$ cooling ages are plotted at their closure temperatures (T_c) with blue vertical bars on the temperature-time (T-t) line representing the present erosion surface (starting depth: 15 km). Modeling results most relevant to the structural levels of this study lie between the 15 km (dotted line) and 20 km (dashed line) T-t curves. Numbered melting reactions in figure A are given in the text, and shaded areas correlate with melt regions in figure 15. White circles and arrowed ellipses in (A) represent melting and deformation events D1 – D4, and are superimposed on these T-t curves at the times dated by zircons in this study; these data are not used to constrain the positions of these curves. Ellipses indicate that melts sampled as dikes and dated at the present erosion level were generated at deeper structural levels. Two double arrows in the late Permian show that while D4 deformation was still operating at upper amphibolite facies metamorphic conditions in the structurally relatively deep Lyme dome, deformation at higher structural levels of the Honey Hill – Lake Char fault system (fig. 3) would occur at lower amphibolite to greenschist facies.

definitely after the D1 event as rare garnets contain inclusion trails of the S1 foliation (fig. 16).

The next event, D3, was one of intrusion of Westerly-type granites. These dikes are straight-walled, and undeformed (fig. 8A), and were thus emplaced from a deeper

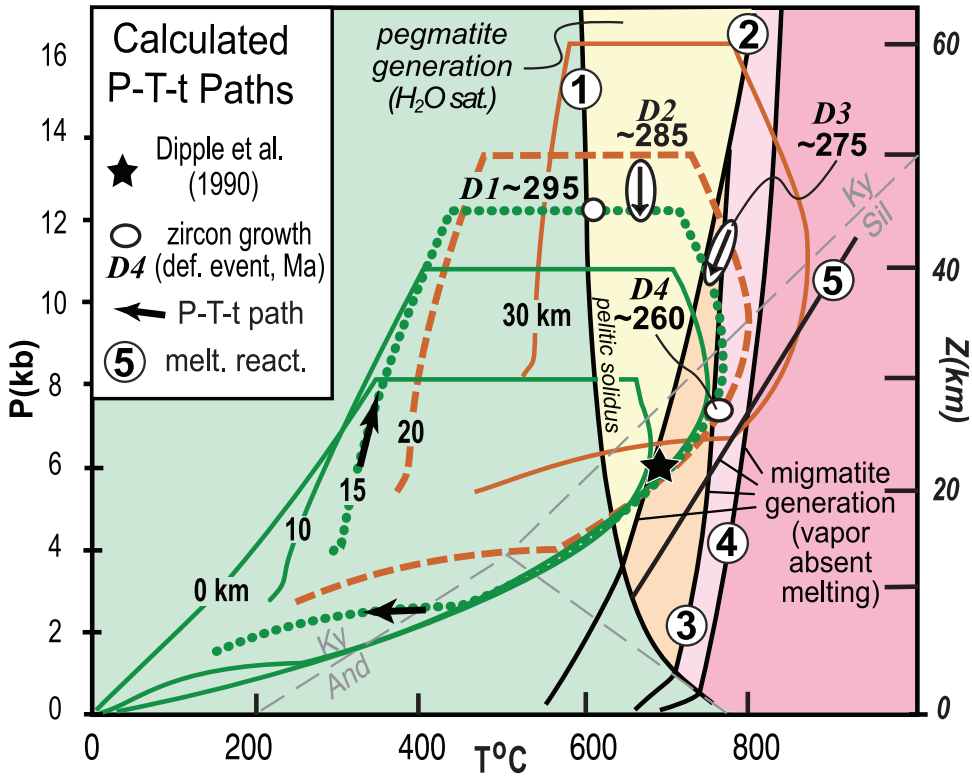

Fig. 15. P-T-t paths for rocks of coastal Connecticut (from Wintsch and others, 2003) showing the P-T conditions of melting and deformation events D1 – D4, using thermal modeling results from figure 14. Melt reactions and sources are described in the text. The validity of the modeled P-T-t paths is supported by their successful prediction of (1) partial melting events D1 through D4, (2) the occurrence of relict kyanite (Lundgren, 1967), and the lack of cordierite (produced below reaction curve 5), and (3) the intersection of the P-T point of Dipple and others (1990).

level at ca. 275 Ma. This is indicated schematically by arrowed ellipses in figures 14 and 15. The drop in (confining) pressure of ca. 200 Mpa is consistent with the fracturing of the host gneisses to produce the cross-cutting dike structures. It is probable that heat was advected into these rocks by the ascent of these magmas, as shown by ages of crystallization of monazite in some rocks, and overgrowth ages on some zircons.

The youngest event in these rocks, D4, was marked by the pervasive intrusion of the youngest pegmatites in these rocks (for example fig. 4D). This event is probably recorded by the crystallization of monazite in both D2 pegmatites and D3 Westerly-like granites (see table 2). This ca. 265 Ma event plots at or near peak temperature conditions of the thermal event of figure 14A, but significantly shows a dramatic drop in pressure to about 700 Mpa. This considerable lowering of confining pressure together with the high fluid (magmatic) pressure undoubtedly contributed to the lowering of rock strength that led to the apparent brittle behavior of the rocks.

Tectonic Model

The results presented here, including U-Pb geochronology on zircon and monazite coupled with structural analysis of rocks in the area of the Lyme dome, lead to a refined, multi-stage model for the Alleghanian orogeny in southern New England (fig. 17). This model identifies the age of intrusive rocks along with age constraints and possible source of metasedimentary rocks in the core of the dome and links the

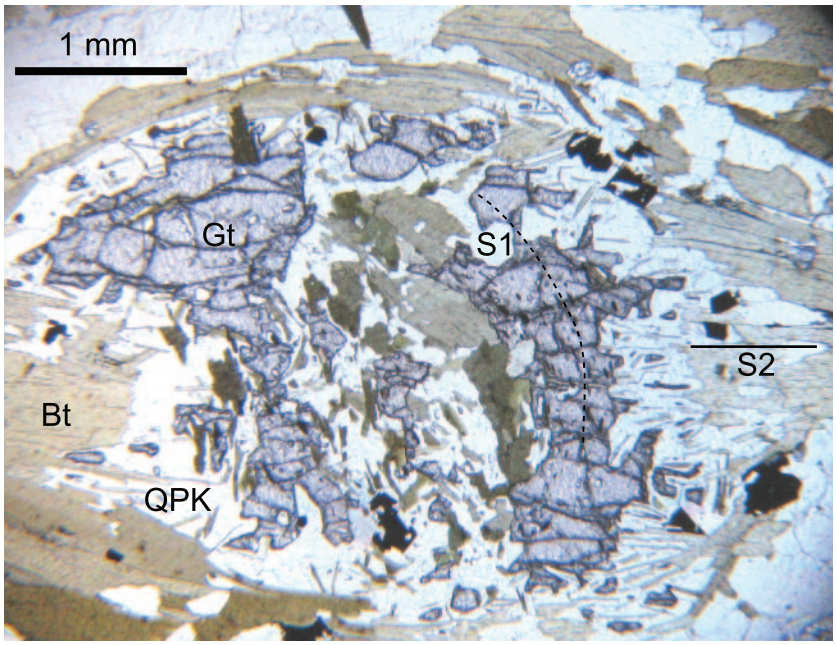

Fig. 16. Photomicrograph of garnet poikiloblast in the Old Lyme Gneiss. Garnet contains S1 inclusion trails (dashed line) and overgrowths in the plane of S2 (solid line) suggesting it grew during or subsequent to D2 deformation. Abbreviations: Gt – garnet, Bt – biotite, QPK – intergrown quartz, plagioclase, and K-feldspar. Photographed in plane light at 2.5 X.

absolute and relative timing of deformational and thermal events of the Alleghanian orogeny including anatexis, dome formation, and widespread decompression melting.

Neoproterozoic Events

Detrital zircon geochronology suggests that the deposition of the metasedimentary rocks in the core of the Lyme dome took place after ca. 925 Ma but before intrusion of the granite and granodiorite at ca. 620 Ma. Zircon age populations of ca. 1060 to 925, 1250 to 1130, 1500 to 1300, 1900 to 1700, and 2125 to 2000 Ma broadly correlate with ages from either Laurentian, Amazonian, or Baltic crust, so by themselves are not uniquely indicative of provenance. Archean detrital zircons are distinctly lacking from our data set, which does not fit a purely Amazonian or Baltic source (Van Staal and others, 1996; Thompson and Bowring, 2000; Barr and others, 2003). Van Staal and others (1996) noted that Gander basement rocks in New Brunswick and Newfoundland best fit a western Amazonian provenance, and that the existence of Grenvillian ages there did not necessarily mean a Laurentian provenance because similar ages occur in Amazonia. Furthermore, Pb and Nd isotopic data from Neoproterozoic igneous rocks in the Clinton and Lyme domes (Aleinikoff and others, 2007) are distinct from Laurentian crustal signatures and are more similar to Ganderian signatures, thus providing evidence that the Old Lyme Gneiss was not derived from Laurentia.

U-Pb zircon ages from granite and granodiorite gneiss in the core of the Lyme dome support a significant intrusive event at ca. 620 to 611 Ma (fig. 17A). These intrusive rocks post-date a relict layer-parallel foliation in the metasedimentary and metavolcanic rocks that is interpreted as bedding (S0). The intrusions may have originated as large sills or sheet-like bodies, but due to subsequent intense Paleozoic

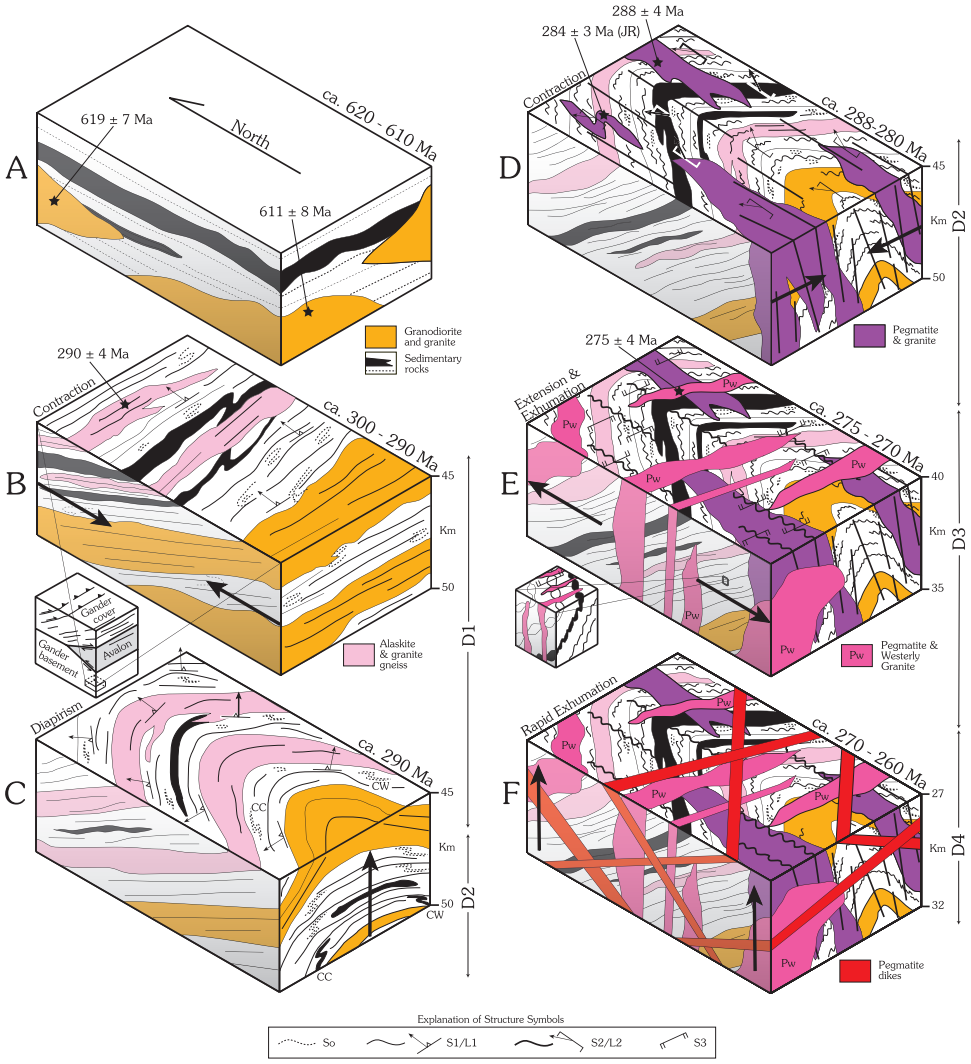

Fig. 17. Block diagrams showing a multi-stage model for the evolution of the Lyme dome. In all diagrams, the locations of U/Pb zircon ages are shown by stars. Depth estimates on the right side of each block are from thermal modeling results (figs. 14 and 15). (A) Neoproterozoic granodiorite and granite intrude protolith sedimentary rocks of the Neoproterozoic Old Lyme Gneiss. The intrusive rocks will later become the orthogneisses at Johnnycake Hill, Lord Hill, and Becket Hill. (B) Regionally penetrative D1 deformation produces mylonitic fabrics, S1 gneissosity, down plunge F1 fold axes, and L1 mineral lineations at aluminosilicate-orthoclase metamorphic conditions. Approximate principal stress direction is north-south contraction (black arrows). Migmatite, alaskite, and granite gneiss intrude in the plane of S1 during partial melting. These conditions may have developed as the Avalon terrane in the Selden Neck block tectonically wedged Gander cover from Gander basement (inset diagram). Regional tilting of the foliation occurred prior to dome-stage folding, or at the very onset of doming. (C) Incipient dome-stage deformation late in D1 or early in D2 deformed S1 and produced radial F1/L1 lineations, with rare F1 fold axes showing core-up fold rotation senses during diapiric ascent (CC, clockwise, CW – counterclockwise). The principal stress direction is vertical diapiric ascent. (D) Continued dome-stage deformation produced S2 foliation axial planar to the dome with NNE plunging F2 fold axes, and L2 mineral lineations. The S2 foliation cuts migmatitic pegmatites and the Joshua Rock Granite Gneiss (JR) that were continually produced during partial melting at second sillimanite conditions. Dome-stage deformation mechanisms switch from diapirism to horizontal contraction. (E) Boudinage and S3 foliation form during D3 as a result of regional crustal uplift, extension, and exhumation. Decompression melts fill the voids created during extensional deformation. Some Westerly Granite and granite pegmatite dikes preferentially intrude along the plane of S3. Inset diagram shows detail of intrusion in boudin necks. (F) Post-tectonic, tabular, gently dipping cross-cutting dikes of granite pegmatite intrude during D4 rapid exhumation and vertical failure of the crust. Zircon and monazite record uplift of the crust to below closure temperatures by ca. 260 Ma. Finally, locally preserved, static retrograde mineral assemblages form at greenschist facies during continued cooling.

deformation, it is difficult to unequivocally state what the original shapes of the intrusions may have been.

Paleozoic Events

Igneous and metamorphic zircon and monazite geochronology, geologic mapping, and structural analysis suggest a link between at least three major Early Permian deformational events associated with Alleghanian orogeny in the Lyme dome area. The events include D1 syn-tectonic migmatization and anatexis during regional foliation development at ca. 290 Ma, dome-stage deformation and uplift from late D1 to D2 at ca. 288 to 280 Ma, and extension and intrusion during D3 at ca. 275 to 270 Ma. Brittle tectonic and thermal activity associated with late granitic dikes continued to at least 259 Ma. These events are summarized in figure 17 and generally involved contraction from D1 to D2, extension during D3, and late tectonic intrusion during exhumation.

Syn-tectonic migmatization and partial melting.—Initial development of the regionally dominant foliation (S1) took place during sillimanite-(or kyanite)-orthoclase metamorphic conditions. Modeling shows that the relic kyanite identified by Lundgren (1967) was probably pervasive at this time (fig. 15). Deformation (D1) produced gneissic fabric and L1 mineral lineations consisting of upper amphibolite facies mineral assemblages. Partial melting accompanied this early high-grade metamorphism probably during H_20-saturated minimum melting (reaction 1) and by muscovite dehydration reactions (reaction 2; Lundgren, 1966a). Regionally, muscovite-poor lithologies may have experienced limited anatexis (McLellan and others, 1993). At this time, early stromatic migmatite developed in metasedimentary rocks from anatectic melts predominantly in the plane of S1 (perhaps by filter pressing, McLellan and others, 1993), and locally as leucocratic segregations along older compositional layering (fig. 11A). Subsequently foliated alaskite and granite gneiss intruded at ca. 290 Ma (sample OL291) associated with syn-tectonic migmatitization in the plane of S1 (fig. 17B).

Sub-parallel down-dip F1 fold axes and L1 mineral lineations suggest high strain in a roughly orthogonal environment. Although deformed, the general trend of L1 and F1 suggests an overall relative north-south transport direction. Regionally, this transport direction has been interpreted as the earliest phase of Alleghanian deformation. Wintsch and others (1990, 1992, 1993, 1998, 2001, 2003) attributed this transport and deformation to thrust-nappe tectonics, but this timing is a bit later than predicted by our modeling. Coleman and others (1997) and Wintsch and others (1998) reported top to SSW at ca. 307 to 305 Ma for this period of thrust motion and related it to local D1 structures in the Bronson Hill terrane, northwest of the Lyme dome. This timing fits the modeling perfectly (fig. 14). Lundgren (1966a) associated this early metamorphism with crustal heating, and Wintsch and others (2003) suggested that this early heating was due to thrust loading which eventually contributed to melt-weakening and faulting in and around the Lyme dome (Wintsch and others, 2005c).

During D1, major faults were active between the Selden Neck block and Lyme dome block. Rocks of the Merrimack terrane are preserved in the Hunts Brook slice which represents a major crustal boundary between the Avalon and Gander terranes. Losh and Bradbury (1984) proposed underthrusting of Avalon along the Honey Hill – Lake Char fault system during this early deformation. Wintsch and others (1990) suggest that the rocks in the Lyme dome moved WNW under the Selden Neck block along a detachment called the Hunts Brook fault zone, and that final emplacement of the thrust slices deformed the mylonites in the fault zone and led to formation of the Lyme dome. Wintsch and others (2005a, 2005c) updated their model stating that the position of the Gander zone rocks in the Lyme dome, structurally beneath the Avalon zone rocks in the Selden Neck block, required that Avalon acted as a wedge, separating Gander metasedimentary cover rocks from the basement on which they had been

deposited. In the wedge model, rocks in the Lyme dome are Gander basement and rocks of the Merrimack terrane are Gander metasedimentary cover (fig. 17B inset).

F1 fold axes show a slightly divergent pattern across the Lyme dome suggesting a somewhat radial pattern (fig. 10). In the core of the dome the fold axes plunge to the NE. On the western limb, the fold axes plunge to the west. On the north side of the dome the axes plunge to the NNW, and on the SE limb the axes plunge to the SSE. In the NE part of the dome the F1 fold axes do not show a consistent radial pattern. D1 mineral lineations show a similar pattern, suggesting somewhat radially divergent elongation. F1 fold rotation senses (fig. 10), although limited, are consistent with core-up relative motion (fig. 17C). Fold rotation sense alone is somewhat equivocal, however, because observed outcrop-scale folds may be, (1) parasitic to larger unseen folds with opposite rotation senses, or (2) rotation senses on the flanks of domes may give opposing shear senses due to changing deformation mechanisms (Whitney and others, 2004; Burg and others, 2004). We, therefore, interpret the rotation senses on minor F1 folds cautiously. Nonetheless, from our data it is possible to conclude that the apparent rotation of F1 fold axes, combined with the radial distribution of F1 and L1 linear elements, are indicative of radial flow as a function of late D1 diapiric uplift (Whitney and others, 2004).

Our data also bear on the issue of whether the Lyme dome formed primarily by diapirism. The Stony Creek dome to the west may have been formed in part by diapirism because of gently dipping foliation in the core, progressive change from L-fabrics to S-fabrics from core to margin, radial lineation patterns, and progressive change from plane strain to flattening from core to margin (McLellan and Stockman, 1985). In the Lyme dome, planar S-fabrics also become more penetrative away from the core of the dome towards the faults in the Hunts Brook slice. The dip of S1 foliation, however, does not show a pattern consistent with flattening in the core as expected with diapiric uplift (Whitney and others, 2004). Figure 18 shows modeled dip values and S1 form-lines around the Lyme dome using inverse distance weighting for both strike and dip values. The strike formlines show that the S1 foliation is not simply folded into a symmetrical dome-like pattern, but rather it contains small-scale folds due to subsequent deformation during D2. Modeled dip values show that the core region contains both steep and gentle dips, with gentle dips ($< 40°$) more common in the northern part of the dome, and steep dips ($< 50°$) more common in the southern core and flanks of the dome. Thus, the dome cannot be explained just by simple diapirism, but must also involve later folding, as shown by the map pattern.

Dome-stage folding and uplift.—Aluminosilicate-orthoclase metamorphic conditions that started during D1 continued through D2 as indicated by second sillimanite mineral assemblages in L2 lineations parallel to F2 fold axes (fig. 12). Granitic pegmatite intruded across the S1 foliation during D2. Locally, the S2 foliation is found in the granitic pegmatite, and this pegmatite yields a U-Pb zircon age of 288 ± 4 Ma. Pegmatite magma generation at this stage generally does not appear to have a preferred orientation, but is widespread throughout the dome. The Joshua Rock Granite Gneiss is also deformed by D2 fabrics and yielded an age of 284 ± 3 Ma, suggesting that D2 deformation spanned a period from approximately 288 to 280 Ma. Thus the time lapse during D1 and D2 is less than 10 m.y.

By D2 time (fig. 17D), L2 mineral lineations and F2 fold axes show generally consistent orientations to the NE, and do not show a radial pattern (fig. 12). Parasitic F2 folds are consistent with development by flexural flow with flanks of the anticline up relative to the core; this orientation is the opposite of F1 fold rotation senses. The radial D1 linear elements and tentative core-up F1 fold rotation senses suggest, therefore, that diapiric uplift began late in D1 (ca. 290 Ma) but was completed by D2 ($>$280 Ma) when horizontal stresses, not vertical, dominated in the development of F2 folds and S2 foliation. Thus, uplift and doming started late in D1 and continued into

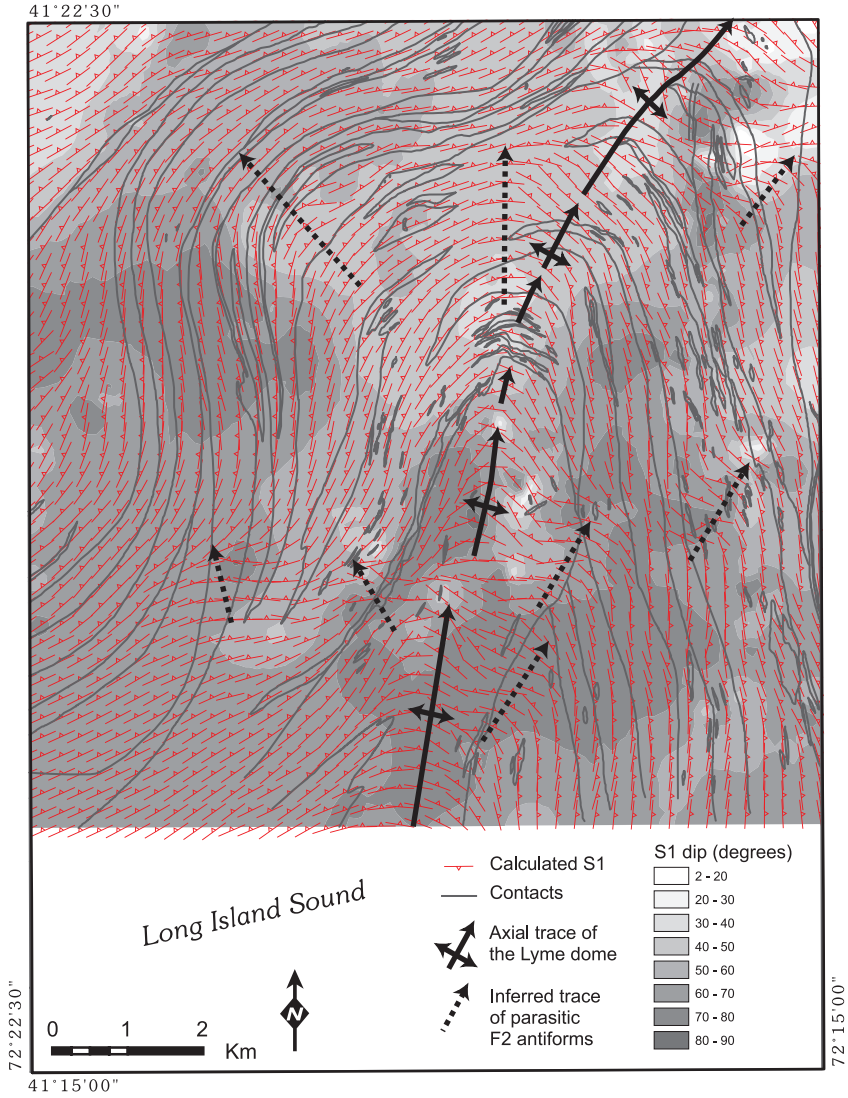

Fig. 18. Form-line map of S1 showing modeled strike direction (symbols) and dip value (grayscale grid). Calculated strike and dip values were interpolated by inverse distance weighting analyses of 698 S1 measurements. The model results indicate that the dome is not a simple antiform, but consists of smaller parasitic antiforms on the flanks of the main trace of the dome. Steep dip values in the core of the dome show that the dome is a composite structure involving interference folding during D2, and not just simple flattening as would be expected by diapirism.

D2, but the apparent dome-forming mechanisms changed from diapirism with vertical dominated flow to contraction with horizontal dominated flow between 290 and 280 Ma.

Hypidiomorphic textures and miarolitic cavities in the Stony Creek dome, similar to those in migmatitic leucosomes at Old Lyme Shores (fig. 3) have been interpreted to indicate rapid decompression during peak metamorphism (McLellan and others, 1993). Similar textures occur throughout the post-S1 leucocratic granitic migmatites in the Lyme dome. Thus, rapid decompression began sometime after D2 and dome-stage

deformation, in other words after ca. 280 Ma. The thermal model also predicts that this exhumation began at ca. 280 Ma (fig. 14).

Extension.—D3 structures, including boudinage, record late horizontal extension with a preferred NNW direction. Granitic pegmatite intrudes across the grain of S1, S2, and the Lyme dome in a generally preferred NNE-SSW direction, along the planes of the S3 cleavage and in extensional zones in boudin necks. More randomly oriented tabular Westerly Granite dikes post-date D3 fabrics in the Lyme dome area, but regionally and with dikes of Narragansett Pier Granite, show a preferred E-W trend (Zartman and Hermes, 1987; Hozik, 1988; Goldsmith, 1988). Emplacement of the Westerly Granite dike at Point O'Woods suggests that preferred NNW D3 extension was active, and perhaps concluded, by ca. 275 Ma.

On the basis of discordias projected through multi-grain fractions of zircon from two samples of Westerly Granite, (including abraded splits with Paleoproterozoic ages), Zartman and Hermes (1987) inferred that the Westerly was derived from Archean crust of the West African shield. They also consider the possibility that the inheritance was due to incorporation of detrital zircons, themselves derived from Archean sources. The oldest $^{207}Pb/^{206}Pb$ ages of abraded zircon in the Zartman and Hermes (1987) study are 1.95 and 2.07 Ga; these ages are similar to the oldest detrital zircons in quartzite from the Old Lyme Gneiss (sample OL096; table 1). We suggest that the Westerly Granite was locally derived from Neoproterozoic metasedimentary rocks of Gander basement. We found no evidence for an Archean source.

Exhumation.—Late, randomly oriented but gently dipping pegmatite dikes record a final stage of intrusion, and a switch from NNW extension to vertical unloading. Metamorphic monazite and zircon rims record crystallization ages of ca. 259 Ma that are indistinguishable from amphibole cooling ages of ca. 260 Ma (Wintsch and others, 1992). These ages show that, by the latest Permian, anatectic conditions had ceased and all rocks had become completely crystallized. Small amounts of lower amphibolite and greenschist facies static overgrowth retrograde mineral assemblages including chlorite and muscovite after biotite, garnet, sillimanite, and K-feldspar record crustal uplift at still lower temperatures, and thus shallower depths.

Extensional fabrics with associated migmatitic infilling and late randomly oriented cross-cutting dikes suggest horizontal failure followed by vertical failure of the rock mass (Brisbin, 1986). Although McLellan and others (p. M-28, 1993) did not report the late D3 fabrics in the Stony Creek dome, they did identify boudin necks and fold hinges as structurally weak zones where younger migmatite developed in small-scale shear zones whose geometry was "controlled by hydraulic failure." Melting by dehydration may have continued to increase the effective pressure and led to rock failure (Brisbin, 1986; McLellan and others, 1993). Wintsch and others (2005c) have suggested that this melt-weakening process started as early as D1, and facilitated early Avalon-Gander terrane juxtaposition where migmatitic liquids at lithostatic pressure apparently lowered the effective stress in the fault zones.

Lundgren (1966a) stated that later emplacement of younger Permian granite such as the Westerly and Narragansett Pier Granites must have been produced from melts derived from deeper levels of the crust because muscovite had already been removed from the rocks during early metamorphism and dehydration-related partial melting. Lundgren recognized that the younger granites post-dated sillimanite-orthoclase conditions and the regional second sillimanite isograd, and suggested that the younger melts could have been derived during the regional metamorphism but from a depth below the isograd. McLellan and others (1993) essentially agreed with Lundgren (1966a) and reiterated the question as to whether the Permian granite pegmatite and Westerly Granite may be related to plutonic heating at depth, thus providing a heat source for younger anatexis at the currently exposed structural level. Lundgren's interpretation may be consistent with ideas that crustal thickening and

heating leads to partial melting of the crust in migmatite gneiss domes (for example, Vanderhaeghe and others, 1999). An alternative hypothesis is that the melts for the younger granites were produced not at significantly deeper levels in the crust but from *in situ* melting during rapid uplift and decompression, as suggested by our thermal modeling and for many migmatite dome complexes (Teyssier and Whitney, 2002; Whitney and others, 2004).

Regionally, fault fabrics associated with the Lake Char – Honey Hill (LCHH) fault post-date the peak of metamorphism and older mylonites in the fault zone. Lundgren (1963), Dixon and Lundgren (1968), and Goldstein (1982, 1989, 1994, 1998) show that LCHH was active during Permian extension producing normal top to the north or northwest motion as the latest movement phase – this motion post-dates dome formation. Lundgren (1963) noted that the motion on the Honey Hill fault was the youngest tectonic event in the area because the latest fault fabrics cut pegmatite intrusions and were associated with post-peak metamorphic retrogression at lower amphibolite facies. Pulver and others (1997) also recognized Permian to Triassic NW extensional fabrics associated with progressive cooling in the Bronson Hill terrane. Although D3 deformation recorded in the Lyme dome records a similar NNW direction, this D3 extension must pre-date subsequent extension seen in the LCHH fault system and at higher levels of the crust because the late extensional melt and intrusion in the dome occurred at ca. 275 Ma or younger and the Honey Hill fault cuts these young granites and pegmatites (Lundgren, 1963). Furthermore, definitive retrograde D3 fabrics with preferred orientations were not recognized in our study, and instead, trace amounts of retrograde minerals statically overgrew higher grade assemblages when the core of the Lyme dome was at post-D3 crustal depths. Our modeling suggests that the D3 extension recorded in the Lyme dome may reflect the initial onset of the latest regional phase of extensional deformation seen at shallower crustal levels, and thus lower metamorphic grades, such as the LCHH fault system. In southern New England, several workers have demonstrated that extension clearly post-dated early ductile deformation, and supporting isotopic mineral ages for this late extension range from ca. 280 to 210 Ma (O'Hara and Gromet, 1983; Getty and Gromet, 1992; Wintsch and others, 1992, 1998).

Mechanisms of Dome Formation

Migmatite gneiss domes, such as the Lyme dome, are widespread in orogenic belts (Eskola, 1949; Teyssier and Whitney, 2002; Whitney and others, 2004; Yin, 2004). Mechanisms of dome formation may include diapirism, thrust-duplexing, viscosity variations, horizontal buckling, polyphase folding, and crustal extension (Yin, 2004; Whitney and others, 2004; Burg and others, 2004). Natural gneiss domes are commonly a product of several mechanisms, making it difficult to unravel the tectonic history and origin of these features (Yin, 2004; Whitney and others, 2004). Teyssier and Whitney (2002) pointed out the important link between decompression melting, deformation, and gneiss dome formation, especially in diapiric models, and contrasted their model with thermally driven melting as a result of crustal thickening (Vanderhaeghe and others, 1999). Whitney and others (2004) outlined the significant differences between magmatic and migmatitic diapirs. Magmatic diapirs intrude the country rock and their rise is related to viscosity contrasts with the surrounding rock; the Killingworth dome in the Bronson Hill terrane is a local example of a magmatic dome (Wintsch and others, 2005b; Aleinikoff and others, 2007). Migmatitic diapirs have a low viscosity contrast with surrounding rocks and they intrude the host rock only to a limited extent and are deformed with the country rock during ascent (Whitney and others, 2004). These authors also propose that gneiss domes are common in orogenic belts because rapid diapiric ascent of partially molten crust quickly cools at shallower crustal depths, preserving the domal structure and ubiquitous migmatite. The thick

section of multiply foliated, migmatitic gneisses exposed in the Lyme dome has allowed us to identify the combination of mechanisms that contributed to producing this poly-deformed structure.

Our data support a model involving multiple mechanisms of dome formation. Early widespread penetrative foliation development (D1) and high grade metamorphism occurred when the crust was greatly thickened. It is probable that the early over-thickened crust (Getty and Gromet, 1992; Moecher and Wintsch, 1994) was produced by crustal wedging as Avalon separated Gander cover from its basement (Wintsch and others, 2005a). This widespread event led to partial melting and migmatization (fig. 14). Rare radial linear elements preserved late in D1 provide limited evidence that suggests that partial melts were funneled into the dome diapirically, and it began to rise buoyantly, causing decompression melting. Limited migration of the partial melts, and not total evacuation of the system, is shown by the preservation of a significant volume of layer-parallel migmatitic leucosomes formed at this stage (Teyssier and Whitney, 2002). Limited diapirism was interrupted perhaps as Gander and Avalon were halted against a Laurentian backstop (Wintsch and others, 1992, 2005a), causing a shift to folding during D2 and creation of the primary form of the Lyme dome as it appears today. Folding by flexural slip would be facilitated and lubricated on the limbs by continued partial melting at near peak metamorphic conditions. Subsequent extension and the onset of unloading led to preferred intrusion of decompression melts along foliation planes and in boudin necks, and continued unloading produced random to shallowly dipping dikes during late hydraulic failure. Goldstein (1982, 1989) suggested that basement diapirism was associated with late normal faulting and is responsible for warping of the Lake Char – Honey Hill fault system at the top of the Avalon terrane. In the core of the Lyme dome, however, structural evidence for diapirism is restricted to late D1 and early D2 time and clearly pre-dates any late extensional event. Mechanisms for driving the late extension remain unresolved and include gravitational collapse of an over-thickened crust (Getty and Gromet, 1992), change in major plate motion from dextral transpression to sinistral strike slip (Wintsch and LeFort, 1984), NE strike-slip convergence and related NW extension in a releasing bend along a major plate boundary now represented by the Lake Char – Honey Hill fault (Goldstein and Hepburn, 1999), or Mesozoic extension related to early opening of the Atlantic basin (Goldstein, 1998). Our findings show that major contractional plate motion was over by ca. 280 Ma, preferred NW extension was concluded by ca. 275 Ma, and vertically-dominated extension of the crust post-dated the NW extension. Our data support a generally continuous series of Carboniferous to Permian events for Alleghanian tectonics lasting approximately 40 Ma and, therefore, do not support significant Mesozoic extension in the area of the Lyme dome. Through thermal modeling, Fayon and others (2004) concluded that rapid exhumation by gently dipping normal faults in gneiss dome belts does not provide sufficient changes in pressure for rapid decompression melting, and that diapiric ascent of the lower crust may be an alternative mechanism. Once the rocks have risen and cooled sufficiently, low angle normal faults may develop in the upper crust during final exhumation (Fayon and others, 2004). We suggest that the model of Fayon and others (2004) may apply to certain stages in the tectonic evolution of southern Connecticut. In this model, fabrics indicative of diapiric ascent are preserved at the structural level of the Lyme dome during late D1 time. By D3 – D4 time, the crust was rapidly rising to shallower levels, and extensional fabrics dominated over diapiric fabrics at the structural level of the Lyme dome. By D4 time, diapirism in the lower crust, below the structural level of the Lyme dome, may have been driving the regional uplift at the same time extensional normal faulting was taking place along the Lake Char – Honey Hill fault system.

CONCLUSIONS

Neoproterozoic Events

Quartzite and paragneiss in the Lyme dome were deposited in the Neoproterozoic sometime between ca. 925 and 620 Ma. Ages of detrital zircons from quartzite in the Old Lyme Gneiss are consistent with an Amazonian provenance, with the exception that Archean zircons were not found in the quartzite nor as xenocrysts in any of the sampled igneous rocks. Neoproterozoic granite and granodiorite intruded the Neoproterozoic metasedimentary rocks in the Lyme dome area at ca. 620 to 610 Ma.

Alleghanian Orogeny

At least four major early Permian deformational events are associated with the Alleghanian orogeny in the Lyme dome area:

- D1 (ca. 290 Ma). Syn-tectonic migmatization and anatexis, including emplacement of alaskite at 290 ± 4 Ma, occurred during regional foliation development and aluminosilicate-orthoclase metamorphic conditions. Detailed structural analysis reveals that the Lyme dome cannot be explained solely by diapirism, but must involve later folding. Locally, rocks of the Selden Neck block in the Avalon terrane may have wedged between Gander terrane cover rocks of the Merrimack terrane and Gander basement in the core of the Lyme dome.
- D2 (ca. 290 – 280 Ma). Rare structures indicative of diapiric uplift of the Lyme dome formed late in D1 and were completed by D2 when horizontal WNW contractional stresses dominated over vertical stresses. D2 deformation folded the regional S1 foliation into the current form of the Lyme dome. Upper amphibolite facies L2 mineral lineations demonstrate that aluminosilicate-orthoclase metamorphic conditions that began during D1 continued through D2. Migmatization continued and syn-tectonic D2 granite pegmatite (288 ± 4 Ma) and the Joshua Rock Granite Gniess (284 ± 3 Ma) intruded at this time.
- D3 (ca. 280 – 275 Ma). North-northwest extension led to granitic pegmatite intrusion along S3 cleavage planes and in extensional zones in boudin necks during hydraulic failure. Intrusion of a Westerly Granite dike at 275 ± 4 Ma, suggests that D3 extension was active, and perhaps concluding, by ca. 275 Ma.
- D4 (ca. 275 – 260 Ma). Late-tectonic randomly oriented but gently dipping pegmatite dikes record a final stage of intrusion, and vertical unloading and exhumation. Monazite and metamorphic zircon rim ages record this event at ca. 259 Ma, after which retrograde mineral assemblages record minimal crustal movement to shallower depths. Diapiric ascent at this time is ruled out at the structural level of Lyme dome, because any structural evidence for diapirism is restricted to late D1 and early D2 time and pre-dates any late extensional event. Ongoing diapirism in the lower crust however, below the level of the Lyme dome, may explain regional crustal uplift of the entire basement complex and extensional normal faulting at shallower crustal depths.

Tectonic Model

Our findings generally support, with some revision, the overall timing of Alleghanian tectonic activity identified at higher structural levels in southeastern New England presented by Wintsch and Lefort (1984), Wintsch and Sutter (1986), Getty and Gromet (1992), and Gromet and others (1998). Alleghanian events involved Late Carboniferous loading and early Permian high-grade ductile deformation from ca. 305 to 290 Ma, dome-stage folding from ca. 290 to 280, felsic magmatism from ca. 290 to 275 Ma, and extension and exhumation from ca. 275 to 260 Ma. In fact, this work helps to reconcile apparent conflicting interpretations (thrust faulting or normal faulting) by demonstrating that prograde loading and thrusting was followed by retrograding exhumation, in part, by normal faulting of rocks in the hanging wall of the Lake Char –

Honey Hill fault zone. This sequence of tectonic events evolved throughout the late Paleozoic. We have found no evidence for Acadian metamorphism or deformation in these rocks.

Discrete deformational phases of the Alleghanian orogeny, recognized by structural analysis, mapping, and geochronology support a multi-stage process for the evolution of the Lyme dome. The evolution of the Lyme dome involved D1 mylonitization and migmatization during north-directed contraction, late D1 diapirism, D2 migmatization during WNW contraction with associated flexural flow and fold interference, D3 NNW horizontal extension, and final late-tectonic D4 vertical extension and exhumation.

ACKNOWLEDGMENTS

We thank Joe Wooden (U. S. Geological Survey) for help with SHRIMP analyses. Ezra Yacob of the U. S. Geological Survey in Denver, Colorado helped with mineral separations. Special thanks go to Scott Southworth, Nicholas Ratcliffe, Lawrence Lundgren, and Craig Dietsch for their helpful suggestions and critical reviews of this paper. Field discussions with Thomas Armstrong were helpful in the initial phase of this investigation. Thanks also go to Byron and Janet Stone for their gracious hospitality during field work. This work was supported by the USGS National Cooperative Geologic Mapping Program and by NSF grant EAR-0510293 awarded to Robert Wintsch and Michael Dorais.

Appendix

Zircon and monazite were extracted from rock samples collected at outcrops in the Old Lyme and Montville quadrangles using standard mineral separation techniques including crushing, pulverizing, Wilfley Table, magnetic separator, and heavy liquids. For igneous rocks, individual grains of each mineral were handpicked; detrital zircons from a quartzite sample were sprinkled onto double-stick tape. All zircons were mounted in epoxy, ground to nearly half-thickness using 1500-grit wet-dry sandpaper, and polished using 6μm and 1μm diamond suspension. All grains were photographed in reflected and transmitted light. Compositional zoning of zircon was imaged in cathodoluminescence (CL) whereas zoning in monazite is shown by backscattered electrons imaging (BSE).

Zircon and monazite were analyzed on the USGS/Stanford sensitive high resolution ion microprobe-reverse geometry (SHRIMP-RG) in Palo Alto, California. The analytical procedures for SHRIMP U-Pb dating follow methods described in Williams (1998). The primary oxygen ion beam, operated at about 4 to 6 nA for SHRIMP-RG, excavated an area of about 25 to 30μm in diameter to a depth of about 1 μm. The spectrometer magnet was cycled through the mass stations six times per analysis for igneous zircon and monazite, and four times for detrital zircons. Elemental fractionation was corrected by analyzing mineral standards of known age every fourth analysis, including: (1) zircon standard R33 (419 ± 1 Ma; Black and others, 2004), and (2) monazite standard 44069 (425 ± 1 Ma; Aleinikoff and others, 2006). Calculated concentrations of Pb and U are believed to be accurate to about 10 to 20 percent.

U-Pb isotopic data from zircon and monazite were reduced and plotted using the Squid and Isoplot/Ex programs of Ludwig (2002, 2003). Common Pb in zircon and monazite is corrected using model Pb isotopic compositions from Stacey and Kramers (1975). Corrected data for zircon are plotted on $^{238}U/^{206}Pb$-$^{207}Pb/^{206}Pb$ concordia diagrams (Tera and Wasserburg, 1972) to visually assess the degree of discordancy of each data point. Ages for igneous rocks are determined by calculating the weighted average of $^{206}Pb/^{238}U$ ages (for Paleozoic rocks). Nearly all analyses of zircon and monazite have very low common Pb contents (common ^{206}Pb is mostly less than 0.2% of total ^{206}Pb, table 1) so that the individual age of each spot analysis is quite insensitive to the common Pb correction. Weighted average calculations of $^{206}Pb/^{238}U$ ages incorporate both the 2-sigma external spot-to-spot error of the standard and the 2-sigma error of the mean of the standard (Ludwig, 2003). All errors for weighted average ages are reported at the 95 percent confidence limit. For detrital zircons, age data that are greater than about 10 percent are excluded from the Relative Probability plot. To construct the plot, we use $^{206}Pb/^{238}U$ ages for grains younger than ca. 1300 Ma and $^{207}Pb/^{206}Pb$ ages for grains older than ca. 1300 Ma.

References

Aleinikoff, J. N., and Stoeser, D. B., 1989, Contrasting zircon morphology and U-Pb systematics in peralkaline and metaluminous post-orogenic granite complexes of the Arabian Shield, Kingdom of Saudi Arabia: Chemical Geology (Isotope Geoscience Section), v. 101, p. 198–206.

Aleinikoff, J. N., Schenck, W. S., Plank, M. O., Srogi, L., Fanning, C. M., Kamo, S. L., and Bosbyshell, H., 2006, Deciphering igneous and metamorphic events in high grade rocks of the Wilmington Complex, Delaware: Morphology, CL and BSE zoning, and SHRIMP U-Pb geochronology of zircon and monazite: Geological Society of America Bulletin, v. 118, n. 1–2, p. 39–64.

Aleinikoff, J. N., Wintsch, R. P., Tollo, R. P., and Unruh, D. M, 2007, Ages and origin of the Killingworth dome, south-central Connecticut: Implications for the tectonic evolution of southern New England: American Journal of Science, v. 307, p. 63–118.

Barr, S. M., and Hegner, E., 1992, Nd isotopic compositions of felsic igneous rocks in Cape Breton, Nova Scotia: Canadian Journal of Earth Sciences, v. 29, p. 650–657.

Barr, S. M., Davis, D. W., Kamo, S., and White, C. E., 2003, Significance of U-Pb detrital ages in quartzite from peri-Gondwanan terranes, New Brunswick and Nova Scotia, Canada: Precambrian Research, v. 126, p. 123–145.

Black, L. P., Kamo, S. L., Allen, C. M., Davis, D. W., Aleinikoff, J. N., Valley, J. W., Mundil, R., Campbell, I. H., Korsuch, R. J., Williams, I. S., and Foudoulis, C., 2004, Improved $^{206}Pb/^{238}U$ microprobe geochronology by the monitoring of a trace-element-related matrix effect; SHRIMP, ID–TIMS, ELA–ICP–MS and oxygen isotope documentation for a series of zircon standards: Chemical Geology, v. 205, p. 115–140.

Brisbin, W. C., 1986, Mechanics of pegmatite intrusion: American Mineralogist, v. 71, p. 644–651.

Buma, G., Frey, F. A., and Wones, D. R., 1971, New England granites: trace element evidence regarding their origin and differentiation: Contributions to Mineralogy and Petrology, v. 31, n. 4, p. 300–320.

Burg, J. P., Kaus, B. J. P., and Podladchikov, Y. Y., 2004, Dome structures in collision orogens: Mechanical investigation of the gravity/compression interplay, *in* Whitney, D. L., Teyssier, C., and Siddoway, C. S., editors, Gneiss domes in Orogeny: Geological Society of America Special Paper, v. 380, p. 47–66.

Coleman, M. E., Pulver, M., Byrne, T. B., Kiyokawa, S., Wintsch, R., Davidek, K. L., and Martin, M., 1997, Late Paleozoic shortening and metamorphism within the Bronson Hill Terrain, central Connecticut: Geological Society of America Abstracts with Programs, v. 29, n. 6, p. 231.

Dallmeyer, R. D., 1982, $^{40}Ar/^{39}Ar$ ages from the Narragansett Basin and southern Rhode Island basement terrane; their bearing on the extent and timing of Alleghenian tectonothermal events in New England: Geological Society of America Bulletin, v. 93, n. 11, p. 1118–1130.

Daniels, D. L., and Snyder, S. L., 2004, New England states aeromagnetic and gravity maps and data: A web site for distribution of data: U.S. Geological Survey Open-File Report 2004–1258, http://pubs.usgs.gov/of/2004/1258/index.htm.

Dipple, G. M., Wintsch, R. P., and Andrews, M. S., 1990, Identification of the scales of differential element mobility in a ductile fault zone: Journal of Metamorphic Geology, v. 8, n. 6, p. 645–661.

Dixon, H. R., and Lundgren, L. W., Jr., 1968, Structure of eastern Connecticut, *in* Zen, E., editor, Studies of Appalachian Geology, northern and marine: New York, Wiley Interscience Publishers, p. 219–229.

Dixon, J. M., 1987, Mantled gneiss domes, *in* Seyfert, C. K., editor, The encyclopedia of structural geology and plate tectonics: New York, Van Nostrand Reinhold, Encyclopedia of Earth Science Series, v. 10, p. 398–412.

Eskola, P., 1949, The problem of mantled gneiss domes: Quarterly Journal of the Geological Society of London, v. 104, pt. 4, n. 416, p. 461–476.

Fayon, A. K., Whitney, D. L., and Teyssier, C., 2004, Exhumation of orogenic crust: Diapiric ascent versus low-angle normal faulting, *in* Whitney, D. L., Teyssier, C., and Siddoway, C. S., editors, Gneiss domes in Orogeny: Geological Society of America Special Paper, v. 380, p. 129–139.

Feininger, T. G., 1963, Westerly Granite and related rocks of the Westerly-Bradford area: New England Intercollegiate Geological Conference Guidebook, 55th Annual Meeting, Providence, Rhode Island, 55 p.

——— 1965, Bedrock geologic map of the Ashaway quadrangle, Connecticut-Rhode Island: U. S. Geological Survey Geologic Quadrangle Map GQ-403, scale 1:24000.

——— 1968, The up dip termination of a large dike of Westerly Granite and the regional distribution of the Westerly and Narragansett Pier granites in Rhode Island and Connecticut: U. S. Geological Survey Professional Paper P-0600, p. D181–D185.

Getty, S. R., and Gromet, L. P., 1992, Geochronological constraints on ductile deformation, crustal extension, and doming about a basement-cover boundary, New England Appalachians: American Journal of Science, v. 292, p. 359–397.

Goldsmith, R., 1961, Axial-plane folding in southeastern Connecticut; Article 169, U. S.: Geological Survey Professional Paper P-0424-C, p. C54-C57.

——— 1967a, Bedrock geologic map of the New London quadrangle: U. S. Geological Survey Geologic Quadrangle Map GQ-574, scale 1:24,000.

——— 1967b, Bedrock geologic map of the Niantic quadrangle, New London County: U. S. Geological Survey Geologic Quadrangle Map GQ-575, scale 1:24,000.

——— 1967c, Bedrock geologic map of the Montville quadrangle, New London County: U. S. Geological Survey Geologic Quadrangle Map GQ-609, scale 1:24,000.

——— 1985a, Honey Hill fault and Hunts Brook syncline, *in* Tracy, R. J., editor, Guidebook for fieldtrips in Connecticut and adjacent areas of New York and Rhode Island, New Haven, Connecticut: New England Intercollegiate Geological Conference, 77th annual meeting, State Geological and Natural History Survey of Connecticut, Guidebook n. 6, p. 491–507.

——— 1985b, Bedrock geologic map of the Old Mystic and part of the Mystic quadrangles, Connecticut, New York, and Rhode Island: U. S. Geological Survey Miscellaneous Investigations Series Map I-1524, scale 1:24,000.
——— 1988, Tectonic significance of dikes of Westerly Granite, southeastern Connecticut and southwestern Rhode Island: Northeastern Geology, v. 10, n. 3, p. 195–201.
Goldstein, A. G., 1982, Geometry and kinematics of ductile faulting in a portion of the Lake Char mylonite zone, Massachusetts and Connecticut: American Journal of Science, v. 282, p. 1378–1405.
——— 1989, Tectonic significance of multiple motions on terrane-bounding faults in the Northern Appalachians: Geological Society of America Bulletin, v. 101, n. 7, p. 927–938.
——— 1992, Motion on the Clinton-Newbury and related faults and multiple deformation of the Merrimack Group in eastern Massachusetts; aspects of the Alleghanian Orogeny in southeastern New England, *in* Robinson, P., and Brady, J. B., editors, Guidebook for fieldtrips in the Connecticut Valley region of Massachusetts and adjacent states: New England Intercollegiate Geological Conference 84th annual meeting, University of Massachusetts Geology Department Contribution, v. 66–1, p. 120–131.
——— 1994, A shear zone origin for Alleghanian (Permian) multiple deformation in eastern Massachusetts: Tectonics, v. 13, p. 62–72.
——— 1998, Lake Char-Honey Hill-Clinton Newbury fault system from southern Massachusetts to southern Connecticut; low-angle normal faults in the Northern Appalachians and their tectonic significance, *in* Murray, D. P., editor, Guidebook for fieldtrips in Rhode Island and adjacent regions of Connecticut and Massachusetts, Kingston, RI: New England Intercollegiate Geological Conference, 90th annual meeting, p. A1.1-A1.20.
Goldstein, A., and Hepburn, J. C., 1999, Possible correlations of the Norumbega fault system with faults in southeastern New England, *in* Ludman, A., and West, D. P., Jr., editors, Norumbega fault system of the Northern Appalachians: Geological Society of America Special Paper, v. 331, p. 73–83.
Gregory, H. E., 1906, Manual of the geology of Connecticut: Connecticut State Geological and Natural History Survey Bulletin N. 6, 273 p.
Gromet, L. P., 1989, Avalonian terranes and late Paleozoic tectonism in southeastern New England; constraints and problems, *in* Dallmeyer, R. D., editor, Terranes in the Circum-Atlantic Paleozoic orogens: Geological Society of America Special Paper N. 230, p. 193–211.
Gromet, L. P., Getty, S. R., and Whitehead, E. K., 1998, Late Paleozoic Orogeny in southeastern New England: a mid-crustal view, *in* Murray, D. P., editor, Guidebook for fieldtrips in Rhode Island and adjacent regions of Connecticut and Massachusetts, Kingston, RI: New England Intercollegiate Geological Conference, 90th annual meeting, p. B2.1-B2.19.
Hermes, O. D., and Zartman, R. E., 1985, Late Proterozoic and Devonian plutonic terrane within the Avalon Zone of Rhode Island: Geological Society of America Bulletin, v. 96, n. 2, p. 272–282.
Hermes, O. D., Gromet, L. P., and Murray, D. P. (compilers), 1994, Bedrock geologic map of Rhode Island: Rhode Island Map Series N. 1, University of Rhode Island, Kingston, scale 1:100,000.
Holdaway, M. J., and Mukhopadhyay, B., 1993, A re-evaluation of the stability relations of andalusite: Thermochemical data and phase diagram for the aluminum silicates: American Mineralogist, v. 78, p. 298–315.
Hoskin, P. W. O., and Schaltegger, U., 2003, The composition of zircon and igneous and metamorphic petrogenesis, *in* Hanchar, J. M., and Hoskin, P. W. O., editors, Zircon: Washington, D. C., Mineralogical Society of America, Reviews in Mineralogy and Geochemistry, v. 53, p. 27–62.
Hozik, M. J., 1988, Tectonic implications of the brittle fracture history of the Permian Narragansett Pier Granite, Rhode Island, *in* Bartholomew, M. J., Hyndman, D. W., Mogk, D. W., and Mason, R., editors, Basement Tectonics 8: Characterization and comparison of ancient and Mesozoic continental margins: Proceedings of the Eighth International Conference on Basement Tectonics, v. 8, p. 503–525.
Kerr, A., 1993, Space-time composition relationships among Appalachian-cycle plutonic suites in Newfoundland, *in* Sinha, A. K., Whalen, J. B., and Hogan, J. P., editors, The Nature of Magmatism in the Appalachian Orogen: Geological Society of America Memoir 191, p. 193–220.
Losh, S., and Bradbury, H. J., 1984, Late Paleozoic deformation within the Honey Hill-Lake Char fault zone, southern New England: Geological Society of America Abstracts with Programs, v. 16, n. 1, p. 48.
Ludwig, K. R., 2002, Squid, version 1.05, A user's manual: Berkeley Geochronology Center Special Publication, N. 2, 16 p.
——— 2003, Isoplot/Ex version 3.00, A geochronological toolkit for Microsoft Excel: Berkeley Geochronology Center Special Publication, N. 4, 73 p.
Lundgren, L., Jr., 1963, The bedrock geology of the Deep River quadrangle: State Geological and Natural History Survey of Connecticut Quadrangle Report N. 13, scale 1:24,000.
——— 1966a, Muscovite reactions and partial melting in southeastern Connecticut: Journal of Petrology, v. 7, p. 421–453.
——— 1966b, The bedrock geology of the Hamburg quadrangle: State Geological and Natural History Survey of Connecticut Quadrangle Report N. 19, scale 1:24,000.
——— 1967, The bedrock geology of the Old Lyme quadrangle: State Geological and Natural History Survey of Connecticut Quadrangle Report N. 21, scale 1:24,000.
Lundgren, L., Jr., and Ebblin, C., 1972, Honey Hill Fault in Eastern Connecticut - Regional Relations: Geological Society of America Bulletin, v. 83, n. 9, p. 2773–2794.
Lundgren, L., Jr., Goldsmith, R., and Synder, G. L., 1958, Major thrust fault in southeastern Connecticut: Geological Society of America Bulletin, v. 69, n. 12, p. 1606.
McLellan, E. L., and Stockman, S., 1985, Age and structural relations of granites, Stony Creek area, Connecticut, *in* Tracy, R. J., editor, Guidebook for fieldtrips in Connecticut and adjacent areas of New York and Rhode Island, New Haven, Connecticut: New England Intercollegiate Geological Conference, 77th annual meeting, State Geological and Natural History Survey of Connecticut, Guidebook n. 6, p. 61–114.

McLellan, E. L., Tracy, R. J., Armstrong, T. R., and Miller, S. J., 1993, Migmatites of southern New England; melting metamorphism and tectonics, *in* Cheney, J. T., and Hepburn, J. C., editors, Field Trip Guidebook for the Northeastern United States: New England Intercollegiate Geological Conference 85th annual meeting and 1993 GSA Annual Meeting, v. 1, University of Massachusetts Geology Department Contribution, v. 67, n. 1, p. M1-M29.

Moecher, D. P., and Wintsch, R. P., 1994, Deformation-induced reconstitution and local resetting of mineral equilibria in polymetamorphic gneisses; tectonic and metamorphic implications: Journal of Metamorphic Geology, v. 12, p. 523–538.

Nichols, D. R., 1956, Bedrock geology of Narragansett Pier quadrangle, Rhode Island: U. S. Geological Survey Geologic Quadrangle Map GQ-0091, scale 1:24,000.

O'Hara, K. D., and Gromet, L. P., 1983, Textural and Rb-Sr isotopic evidence for late Paleozoic mylonitization within the Honey Hill fault zone, southeastern Connecticut: American Journal of Science, v. 283, p. 762–779.

Pulver, M. H., Coleman, M. E., Byrne, T., Wintsch, R. P., Kunk, M. J., Boyd, J. L., and Dunnigan, J., 1997, Structure and chronology of a section of the Bronson Hill Terrane; significance for late Paleozoic to early Mesozoic exhumation in south-central New England: Geological Society of America Abstracts with Programs, v. 29, n. 6, p. 231.

Rankin, D. W., Coish, R. A., Tucker, R. D., Peng, Z. X., Wilson, S. A., and Rouff, A.A., 2007, Silurian extension in the upper Connecticut Valley, United States and the origin of Middle Paleozoic basins in the Québec embayment: American Journal of Science, v. 307, p. 216–264.

Rodgers, J., 1985, Bedrock geological map of Connecticut: Hartford, Connecticut Geological and Natural History Survey, Department of Environmental Services, scale 1:125,000.

Salvini, F., 2004, Structural Data Integrated System Analyzer software (DAISY), Dipartimento di Scienze Geologiche, Universita degli Studi di "Roma Tre", Rome, Italy, ftp://ftp.u-cergy.fr/geol/Daisy/.

Skehan, J. W., and Rast, N., 1990, Pre-Mesozoic evolution of Avalon terranes of southern New England, *in* Socci, A. D., Skehan, J. W., and Smith, G. W., editors, Geology of the composite Avalon terrane of southern New England: Geological Society of America Special Paper, v. 245, p. 13–53.

Snyder, G. L., 1964, Petrochemistry and bedrock geology of the Fitchville quadrangle, Connecticut: U. S. Geological Survey Bulletin 1161-I, scale 1:24000.

Spear, F. S., Kohn, M. J., and Cheney, J. T., 1999, P-T paths from anatectic pelites: Contributions to Mineralogy and Petrology, v. 134, p. 17–32.

Stacey, J. S., and Kramers, J. D., 1975, Approximation of terrestrial lead isotope evolution by a two-stage model: Earth and Planetary Science Letters, v. 26, p. 207–221.

Steiger, R. H., and Jäger, E., 1977, Subcommission on geochronology, convention on the use of decay constants in geo- and cosmochronology: Earth and Planetary Science Letters, v. 36, p. 359–362.

Stone, J. R., Schafer, J. P., London, E. H., DiGiacomo-Cohen, M. L., Lewis, R. S., Thompson, W. B., and Stone, B. D., 2005, Quaternary geologic map of Connecticut and Long Island Sound basin, with a section on sedimentary facies and morphosequences of glacial meltwater deposits: U. S. Geological Survey Scientific Investigations Map SIM-2784, scale 1:125,000.

Tera, F., and Wasserburg, G. J., 1972, U-Th-Pb systematics in three Apollo 14 basalts and the problem of initial Pb in lunar rocks: Earth and Planetary Science Letters, v. 14, p. 281–304.

Teyssier, C., and Whitney, D. L., 2002, Gneiss domes and orogeny: Geology, v. 30, p. 1139–1142.

Thompson, M. D., and Bowring, S. A., 2000, Age of the Squantum "Tillite," Boston basin, Massachusetts: U-Pb zircon constraints on terminal Neoproterozoic glaciation: American Journal of Science, v. 300, p. 630–655.

van Staal, C. R., 2005, North America: Northern Appalachians, *in* Selley, R. C., Cocks, R. L. M., and Plimer, I. R., editors, Encyclopedia of Geology: Oxford, United Kingdom, Elsevier, v. 4, p. 81–91.

van Staal, C. R., Sullivan, R. W., and Whalen, J. B., 1996, Provenance of tectonic history of the Gander Zone in the Caledonian/Appalachian Orogen; implications for the origin and assembly of Avalon, *in* Nance, R. D., and Thompson, M. D., editors: Geological Society of America Special Paper, v. 304, p. 347–367.

Vanderhaeghe, O., Teyssier, C., and Wysoczanski, R., 1999, Structural and geochronological constraints on the role of partial melting during the formation of the Shuswap metamorphic core complex at the latitude of the Thor-Odin Dome, British Columbia: Canadian Journal of Earth Sciences, v. 36, n. 6, p. 917–943.

Vielzeuf, D., and Schmidt, M. W., 2001, Melting relations in hydrous systems revisited; application to metapelites, metagreywackes and metabasalts: Contributions to Mineralogy and Petrology, v. 141, p. 251–267.

Walsh, G. J., Scott, R. B., Aleinikoff, J. N., and Armstrong, T. R., 2006, Preliminary bedrock geologic map of the Old Lyme quadrangle, New London and Middlesex Counties, Connecticut: U. S. Geological Survey Open File Report 2006–1296, scale 1:24,000.

Watson, E. B., 1979, Zircon saturation in felsic liquids: Experimental results and applications to trace element geochemistry: Contributions to Mineralogy and Petrology, v. 79, p. 407–419.

Watson, E. B., and Harrison, T. M., 1983, Zircon saturation revisited: temperature and composition effects in a variety of crustal magma types: Earth and Planetary Science Letters, v. 64, p. 295–304.

Whalen, J. B., Jenner, G. A., Currie, K. L., Barr, S. M., Longstaffe, F. J., and Hegner, E., 1994, Geochemical and isotopic characteristics of granitoids of the Avalon Zone, New Brunswick: Possible evidence for repeated delamination events: Journal of Geology, v. 102, p. 269–282.

Whitney, D. L., Teyssier, C., and Vanderhaeghe, O., 2004, Gneiss domes and crustal flow, *in* Whitney, D. L., Teyssier, C., and Siddoway, C. S., editors, Gneiss domes in Orogeny: Geological Society of America Special Paper, v. 380, p. 15–33.

Williams, I. S., 1998, Chapter 1, U-Th-Pb geochronology by ion microprobe, *in* McKibben, M. A., Shanks, W. C., III, and Ridley, W. I., editors, Applications of microanalytical techniques to understanding mineralizing processes: Reviews of Economic Geology, v. 7, p. 1–35.

Williams, I. S., and Hergt, J. M., 2000, U-Pb dating of Tasmanian dolerites: a cautionary tale of SHRIMP analysis of high-U zircon, *in* Woodhead, J. D., Hergt, J. M., and Noble, W. P., editors, Beyond 2000: New Frontiers in Isotope Geoscience, Abstracts and Proceedings, p. 185–188.
Wintsch, R. P., 1979, The Willimantic fault: A ductile fault in eastern Connecticut: American Journal of Science, v. 279, p. 367–393.
Wintsch, R. P., and Aleinikoff, J. N., 1987, U-Pb isotopic and geologic evidence for late Paleozoic anatexis, deformation, and accretion of the late Proterozoic Avalon Terrane, southcentral Connecticut: American Journal of Science, v. 287, p. 107–126.
Wintsch, R. P., and Lefort, J. P., 1984, A clockwise rotation of Variscan strain orientation in SE New England and regional implications, *in* Hutton, D. H. W., and Sanderson, D. J., editors, Variscan Tectonics of the North Atlantic Region: London, Blackwell, p. 245–251.
Wintsch, R. P., and Sutter, J. F., 1986, A tectonic model for the late Paleozoic of southern New England: Journal of Geology, v. 94, p. 459–472.
Wintsch, R. P., Andrews, M. S., and Ambers, C. P., 1990, Thrust napping versus fold napping in the Avalon terrane of southeastern Connecticut, *in* Socci, A. D., Skehan, J. W., and Smith, G. W., editors, Geology of the composite Avalon terrane of southern New England: Geological Society of America Special Paper, v. 145, p. 209–233.
Wintsch, R. P., Sutter, J. F., Kunk, M. J., Aleinikoff, J. N., and Dorais, M. J., 1992, Contrasting P-T-t paths: thermochronologic evidence for a late Paleozoic final assembly of the Avalon composite terrane in the New England Appalachians: Tectonics, v. 11, p. 672–689.
Wintsch, R. P., Sutter, J. F., Kunk, M. J., Aleinikoff, J. N., and Boyd, J. L., 1993, Alleghanian assembly of Proterozoic and Paleozoic lithotectonic terranes in south central New England: new constraints from geochronology and petrology, *in* Cheney, J. T., and Hepburn, J. C., editors, Field Trip Guidebook for the Northeastern United States: New England Intercollegiate Geological Conference 85th annual meeting and 1993 GSA Annual Meeting, v. 1, University of Massachusetts Geology Department Contribution, v. 67, n. 1, p. H1-H30.
Wintsch, R. P., Coleman, M., Pulver, M., Byrne, T., Aleinikoff, J., Kunk, M., and Roden-Tice, M., 1998, Late Paleozoic deformation, metamorphism, and exhumation in central Connecticut, *in* Murray, D. P., editor, Guidebook for fieldtrips in Rhode Island and adjacent regions of Connecticut and Massachusetts, Kingston, Rhode Island: New England Intercollegiate Geological Conference, 90th annual meeting, p. C2.1-C2.21.
Wintsch, R. P., Kelsheimer, K. L., Kunk, M. J., and Aleinikoff, J. N., 2001, A new look at the Alleghanian overprint of Acadian metamorphic rocks in southern New England: Evidence from structure, petrology and thermochronology, *in* West, D. P., and Bailey, R. H., editors, Guidebook for geological field trips in New England: Geological Society of America Annual Meeting, Boston, p. V1-V26.
Wintsch, R. P., Kunk, M. J., Boyd, J. L., and Aleinikoff, J. N., 2003, P-T-t paths and differential Alleghanian loading and uplift of the Bronson Hill terrane, south central New England: American Journal of Science, v. 303, p. 410–446.
Wintsch, R. P., Aleinikoff, J. N., Unruh, D. M., and Walsh, G., 2005a, Evidence for tectonic wedging of Avalon terrane rocks into the Gander zone, southern New England: Geological Society of America Abstracts with Programs, v. 37, p. 31.
Wintsch, R. P., Aleinikoff, J. N., Webster, J. R., and Unruh, D. M., 2005b, The Killingworth complex: A Middle and Late Paleozoic magmatic and structural dome, *in* McHone, N. W., and Petersone, M. J., editors, Guidebook for fieldtrips in Connecticut, New Haven, CT: New England Intercollegiate Geological Conference, 97th annual meeting, State Geological and Natural History Survey of Connecticut, Guidebook n. 8, p. 305–324.
Wintsch, R. P., Aleinikoff, J. N., Dorais, M. J., Unruh, D. M., and Walsh, G. J., 2005c, Melt weakening in crustal-scale tectonic wedging, southern New England: EOS Transactions, v. 86, n. 52, p. V21A-0591.
Wintsch, R. P., Aleinikoff, J. N., Walsh, G. J., Bothner, W. A., and Hussey, A. M., 2007, SHRIMP U-Pb evidence for a Late Silurian age of metasedimentary rocks in the Merrimack and Putnam-Nashoba terranes, eastern New England: American Journal of Science, v. 307, p. 119–167.
Yin, A., 2004, Gneiss domes and gneiss dome systems, *in* Whitney, D. L., Teyssier, C., and Siddoway, C. S., editors, Gneiss domes in Orogeny: Geological Society of America Special Paper, v. 380, p. 1–14.
Zartman, R. E., and Hermes, O. D., 1987, Archean inheritance in zircon from late Paleozoic granites from the Avalon Zone of southeastern New England; an African connection: Earth and Planetary Science Letters, v. 82, n. 3–4, p. 305–315.
Zartman, R. E., Hermes, O. D., and Pease, M. H., Jr., 1988, Zircon crystallization ages and subsequent isotopic disturbance events in gneissic rocks of eastern Connecticut and western Rhode Island: American Journal of Science, v. 288, p. 376–402.
Zietz, I., Kirby, J. R., Jr., and Gilbert, F. P., 1974, Aeromagnetic map of Connecticut: U. S. Geological Survey Geophysical Investigations Map GP-897, scale 1:125,000.
Zietz, I., Gilbert, F. P., and Kirby, J. R., 1980, Aeromagnetic map of Connecticut, Massachusetts, New Hampshire, Rhode Island, Vermont, and part of New York: U. S. Geological Survey Geophysical Investigations Map GP-928, scale 1:1,000,000.